Calhoun: The NPS Institutional Archive

DSpace Repository

Theses and Dissertations | 1. Thesis and Dissertation Collection, all items

2018-06

IMPLEMENTATION OF REACTIVE POWER FLOW CONTROL IN A SINGLE-PHASE MICROGRID

Mendoza, Christopher

Monterey, CA; Naval Postgraduate School

http://hdl.handle.net/10945/59553

Downloaded from NPS Archive: Calhoun

http://www.nps.edu/library

Calhoun is a project of the Dudley Knox Library at NPS, furthering the precepts and goals of open government and government transparency. All information contained herein has been approved for release by the NPS Public Affairs Officer.

Dudley Knox Library / Naval Postgraduate School
411 Dyer Road / 1 University Circle
Monterey, California USA 93943

NAVAL POSTGRADUATE SCHOOL

MONTEREY, CALIFORNIA

THESIS

IMPLEMENTATION OF REACTIVE POWER FLOW CONTROL IN A SINGLE-PHASE MICROGRID

by

Christopher Mendoza

June 2018

Thesis Advisor: Giovanna Oriti
Second Reader: Roberto Cristi

Approved for public release. Distribution is unlimited.

THIS PAGE INTENTIONALLY LEFT BLANK

REPORT DOCUMENTATION PAGE			*Form Approved OMB No. 0704-0188*

Public reporting burden for this collection of information is estimated to average 1 hour per response, including the time for reviewing instruction, searching existing data sources, gathering and maintaining the data needed, and completing and reviewing the collection of information. Send comments regarding this burden estimate or any other aspect of this collection of information, including suggestions for reducing this burden, to Washington headquarters Services, Directorate for Information Operations and Reports, 1215 Jefferson Davis Highway, Suite 1204, Arlington, VA 22202-4302, and to the Office of Management and Budget, Paperwork Reduction Project (0704-0188) Washington, DC 20503.

1. AGENCY USE ONLY *(Leave blank)*	**2. REPORT DATE** June 2018	**3. REPORT TYPE AND DATES COVERED** Master's thesis

4. TITLE AND SUBTITLE IMPLEMENTATION OF REACTIVE POWER FLOW CONTROL IN A SINGLE-PHASE MICROGRID	**5. FUNDING NUMBERS**
6. AUTHOR(S) Christopher Mendoza	
7. PERFORMING ORGANIZATION NAME(S) AND ADDRESS(ES) Naval Postgraduate School Monterey, CA 93943-5000	**8. PERFORMING ORGANIZATION REPORT NUMBER**
9. SPONSORING / MONITORING AGENCY NAME(S) AND ADDRESS(ES) N/A	**10. SPONSORING / MONITORING AGENCY REPORT NUMBER**

11. SUPPLEMENTARY NOTES The views expressed in this thesis are those of the author and do not reflect the official policy or position of the Department of Defense or the U.S. Government.

12a. DISTRIBUTION / AVAILABILITY STATEMENT Approved for public release. Distribution is unlimited.	**12b. DISTRIBUTION CODE** A

13. ABSTRACT (maximum 200 words)

Advancements have been made in the field of power electronics and particularly in energy management of microgrids. In this thesis, we present a comparison of two single-phase reactive power control strategies used to achieve a unity power factor with an energy management system in an AC microgrid. The first method measures the root-mean square of both voltage and current and relies on principles derived from the power triangle. The second method is based on the instantaneous reactive power αβ theory normally proposed for three-phase systems. In creating a secondary imaginary orthogonal circuit, this control method can be applied to a single-phase system. The proposed control schemes were designed and validated utilizing a physics-based microgrid model. The model was used in a grid-connected mode scenario with a resistive-inductive load. Once both methods were designed and implemented in MATLAB-SIMULINK, the model behaved as expected for real power. Both control methods were nearly identical in providing reactive power compensation to create unity power factor. Some differences were observed while conducting transient-type testing, but they had negligible impact on the overall operation of the microgrid.

14. SUBJECT TERMS Energy Management System, unity power factor, reactive control, real and reactive power modeling	**15. NUMBER OF PAGES** 65
	16. PRICE CODE

17. SECURITY CLASSIFICATION OF REPORT	**18. SECURITY CLASSIFICATION OF THIS PAGE**	**19. SECURITY CLASSIFICATION OF ABSTRACT**	**20. LIMITATION OF ABSTRACT**
Unclassified	Unclassified	Unclassified	UU

NSN 7540-01-280-5500

Standard Form 298 (Rev. 2-89)
Prescribed by ANSI Std. 239-18

THIS PAGE INTENTIONALLY LEFT BLANK

Approved for public release. Distribution is unlimited.

IMPLEMENTATION OF REACTIVE POWER FLOW CONTROL IN A SINGLE-PHASE MICROGRID

Christopher Mendoza
Commander, United States Navy
BS, Iowa State University, 2001

Submitted in partial fulfillment of the
requirements for the degree of

MASTER OF SCIENCE IN ELECTRICAL ENGINEERING

from the

NAVAL POSTGRADUATE SCHOOL
June 2018

Approved by: Giovanna Oriti
Advisor

Roberto Cristi
Second Reader

R. Clark Robertson
Chair, Department of Electrical and Computer Engineering

THIS PAGE INTENTIONALLY LEFT BLANK

ABSTRACT

Advancements have been made in the field of power electronics and particularly in energy management of microgrids. In this thesis, we present a comparison of two single-phase reactive power control strategies used to achieve a unity power factor with an energy management system in an AC microgrid. The first method measures the root-mean square of both voltage and current and relies on principles derived from the power triangle. The second method is based on the instantaneous reactive power αβ theory normally proposed for three-phase systems. In creating a secondary imaginary orthogonal circuit, this control method can be applied to a single-phase system. The proposed control schemes were designed and validated utilizing a physics-based microgrid model. The model was used in a grid-connected mode scenario with a resistive-inductive load. Once both methods were designed and implemented in MATLAB-SIMULINK, the model behaved as expected for real power. Both control methods were nearly identical in providing reactive power compensation to create unity power factor. Some differences were observed while conducting transient-type testing, but they had negligible impact on the overall operation of the microgrid.

THIS PAGE INTENTIONALLY LEFT BLANK

TABLE OF CONTENTS

LIST OF FIGURES

LIST OF TABLES

THIS PAGE INTENTIONALLY LEFT BLANK

LIST OF ACRONYMS AND ABBREVIATIONS

AC	alternating current
BBC	buck-boost converter
CCM	continuous conduction mode
CONUS	continental United States
CNO	Chief of Naval Operations
DC	direct current
DG	distributed generation
DCM	discontinuous conduction mode
DOD	Department of Defense
DOE	Department of Energy
EMS	energy management system
IEEE	Institute of Electrical and Electronics Engineers
IGBT	insulated gate bipolar transistor
IRP	instantaneous reactive power theory
KCL	Kirchhoff's Current Law
KVL	Kirchhoff's Voltage Law
LPF	low pass filter
OPNAV	Office of the Chief of Naval Operations
PI	proportional integrator
pf	power factor
PWM	pulse-width modulation
RMS	root mean square
USMC	United States Marine Corps
VSI	voltage source inverter

THIS PAGE INTENTIONALLY LEFT BLANK

ACKNOWLEDGMENTS

First and foremost, I would like to express my sincere gratitude to Professors Giovanna Oriti and Roberto Cristi for their continuous support, patience, enthusiasm, and knowledge during this process. Your continued guidance helped me during the research and writing of this thesis. I would like to express my very great appreciation to Dr. Alexander Julian for his valuable and constructive suggestions and willingness to give his time so generously.

I thank my fellow classmates and colleagues Damian Oslebo, Mike Ross, and Alex Baynes for their camaraderie and expertise throughout our time here. I would be remiss if I did not mention Ashley Lawrence: thank you for your contributions and the constant reminder that not everybody is an engineer. Last, no one has been more important to me in this endeavor than members of my family. I would like to thank my parents, whose love and guidance are with me in whatever I pursue.

THIS PAGE INTENTIONALLY LEFT BLANK

I. INTRODUCTION

The demand for cost efficient, cleaner energy sources and reliable electricity is increasingly growing. Yet the current grid and transmission infrastructure at large remain the same. The basic infrastructure of the electric system from the generation of power to the end user, a design and concept that dates back to the 1830s, can be seen in Figure 1.

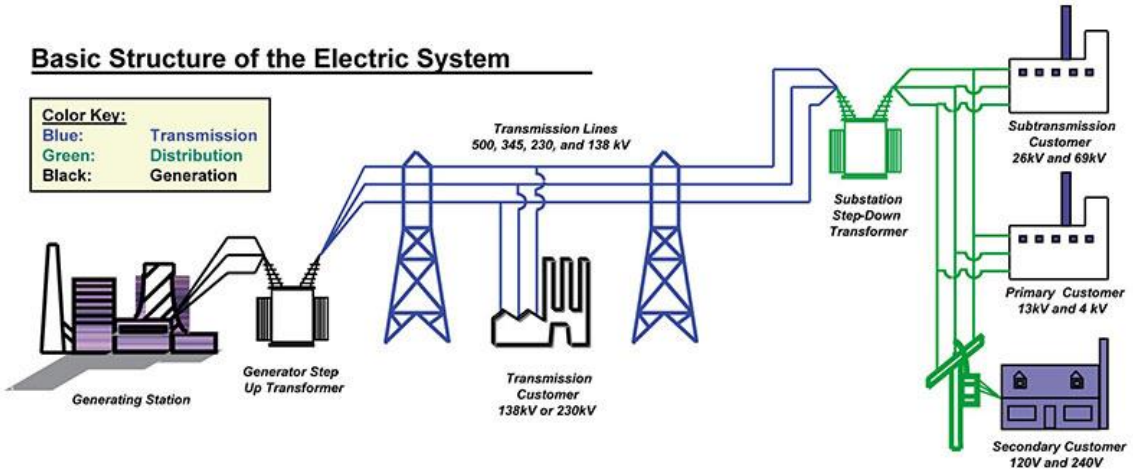

Figure 1. Basic Structure of the Electrical System. Source: [1].

What may not be readily apparent from Figure 1 is how we have painted the landscape of the United States from coast to coast with transmission lines and, in doing so, incurred costly transmission losses and other issues due to such long distances. The transmission and distribution lines "have been called the world's largest machine and part of the greatest engineering achievements of the 20th century," but the 21st century brings new requirements and challenges that need to be incorporated into the current grid system to meet the ever-growing demand for reliable electricity [2].

The Department of the Navy's (DON) Energy Program for Security and Independence acknowledges the current status of the U.S. grid system by setting forth official policy outlining five energy goals, including the utilization of microgrids. The Department of Energy (DOE) defines microgrids as "a group of interconnected loads and

distributed energy resources within clearly defined electrical boundaries that acts as a single controllable entity with respect to the grid. A microgrid can connect and disconnect from the grid to enable it to operate in grid-connected or islanding-mode" [3]. The definition given by the DOE is summarized in Figure 2, in which a generic representation of a microgrid with all critical parts is illustrated.

The Energy Management System (EMS), illustrated in Figure 2, controls the entire microgrid system based on a variety of inputs and feedback values. In addition to managing the microgrid's modes of operation, distributed generation (DG) systems, and other auxiliary functions, different control schemes can be employed to allow for active and reactive power control. These type of control schemes allow the EMS to obtain a unity power factor, creating an optimal efficiency of the system.

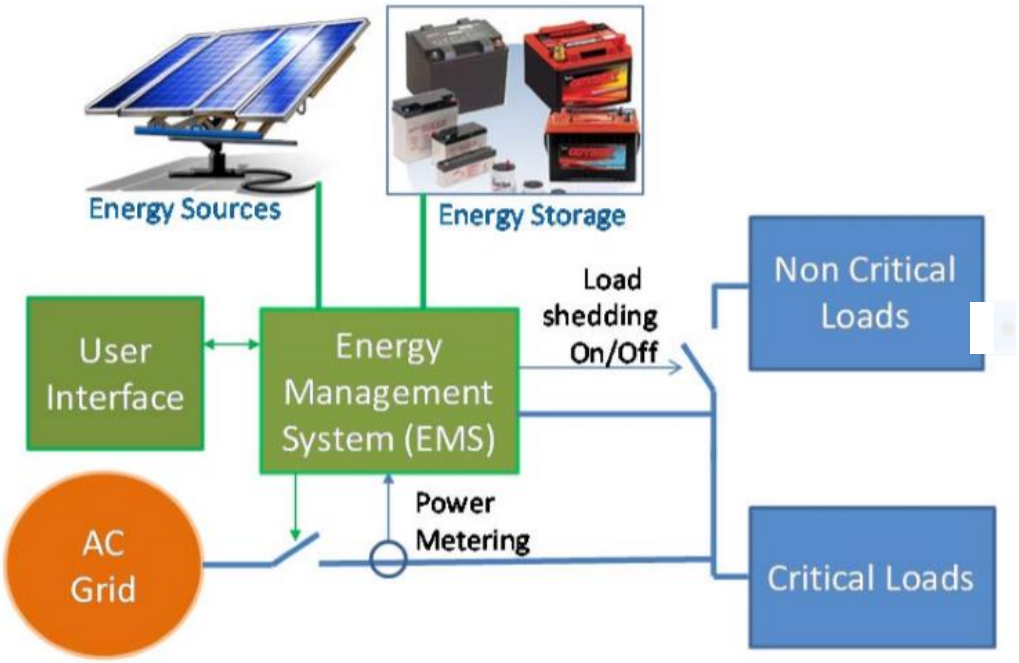

Figure 2. An EMS Connected to the Main Grid and Microgrid. Source: [4].

There are currently 87 U.S. Naval bases within the continental United States (CONUS), not including annexes, recruiting commands, training centers, and overseas shore bases. All sites under U.S. Navy oversight require power from the grid [5]. The U.S.

Navy has released a new Shore Energy Program which states "Energy bills are the single largest cost for Navy installations, reflecting about 28% of Navy's shore budget. The Navy must reduce energy costs to free up scarce budget dollars to support training and fleet operations" [6]. With increased fiscal constraints, all Department of Defense (DOD) entities have taken steps to reduce energy consumption and have developed teams such as the Navy's "Task Force Energy" and the United States Marine Corps (USMC) "Expedition Energy." The capstone guidance for the previously mentioned programs can be found in the Office of the Chief of Naval Operations (OPNAV) instruction 4100.5E, "Shore Energy Management" [7]. This document contains guidance on alternative fuels, reduced energy consumption, microgrids, and many other cost saving energy initiatives for the DON.

As previously described, the current grid system relies on thousands of miles of transmission lines and transformers, creating inefficiencies along the way. The total system inefficiency, according to R. H. Lasseter et al., has to do with the fact that "most existing power plants, central or distributed, deliver electricity to user sites at an overall fuel-to-electricity efficiency in the range of 28–32%. This represents a loss of around 70% of the primary energy." [8]. In addition to transmission losses, the grid is also susceptible to physical, weather, and cyber-attacks. Although not discussed in this thesis, the microgrid concept can contain malicious or unintentional loss of power. In fiscal year 2014, the DOD reported 114 power outages at military instillations that lasted eight hours or more, at a cost of $246,000 per day [9].

The microgrid is not a new concept to the U.S. Navy. In its basic form, the microgrid is a secondary means of power when the primary source fails. All U.S. warships have secondary and, in some cases, tertiary backup sources of power in the event of a loss of main power. This concept is crucial for critical shore installations as well since many shore installations are necessary to meet mission-ready capability requirements. The DOD has used backup generators as a secondary means of power on shore installations, but this strategy has limitations based on the ability to provide fuel for extended use during long-term power outages. Dennis McGinn, Assistant Secretary of the Navy for Installation, Energy and Environment, states that "the Navy and Marine Corps have 41 different diesel generators operating at its bases. Some of them are state-of-the-art, in terms of efficiency

and reliability…the majority of them aren't as reliable as we expected, or as they were guaranteed to be when we bought them" [10].

If all periodic diesel generator maintenance and testing are in compliance with the facilities and manufacturers specifications, then, at best, secondary power is a viable option as a short-term solution. Limitations on length of power outages still exist, which may be a severe issue for a forward deployed base, critical units, or DOD CONUS facilities that are considered as mission critical. In addition to length of power outage concerns, these types of systems are mainly hardwired into a building's network, and depending on the number of critical buildings, may require significant number of diesel generators. In some cases, these diesel generators are not automated and require operator control in the event of a power outage due to weather, utility maintenance, or malicious actions.

The vulnerabilities of the current grid, including malicious and natural disaster, and the calculated risks associated with secondary power are in need of a twenty-first century update. Technological advances in energy storage, cleaner energy sources, power electronics, and power distribution are in alignment with the DOD's initiative to allow our bases to be mission ready and reduce the financial impact of current system inefficiencies. An example of a hypothetical generic base implementing the microgrid system is depicted in Figure 3. As briefly stated earlier, many advancements have been made in the field of power electronics and particularly in energy management of microgrids and their associated DG systems [12]–[14]. In this thesis, we examine a military application of the microgrid, focusing on the EMS that can be used to control a generic base with multiple DG sources and a network of primary and secondary loads, as illustrated in Figure 3.

.

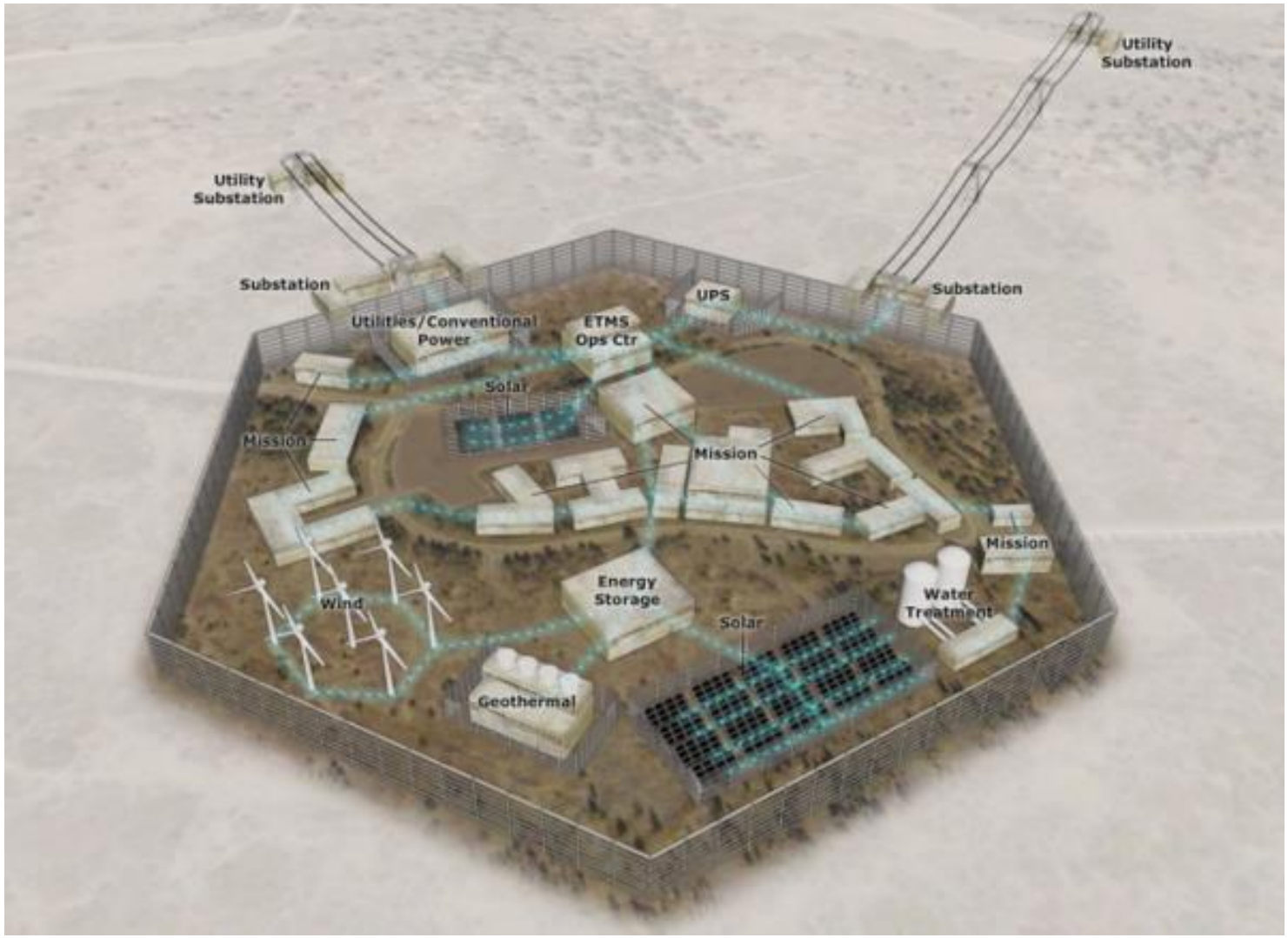

Figure 3. Generic Base Microgrid Implementation. Source: [11].

In the last ten years, several advanced control scheme methods have been introduced as a means to control insertion of reactive power and instantaneous output voltage with zero steady-state error at a design frequency of the converter used in an EMS [15],[16]. These methods include the fast inner-current loop with a slow outer-voltage loop, repetitive controllers, and deadbeat controllers to name a few [17], [18]. In this thesis, we focus on two plausible control schemes: the Instantons Reactive Power (IRP) (αβ) theory control scheme and the root-mean square (RMS) control method. Both techniques allow for reactive power insertion into the grid to create a unity power factor (pf) when the EMS is in grid-connected mode. The importance of keeping a satisfactory pf is that it is a measure of efficiency. In fact, by obtaining a unity pf, the EMS reduces costs as addressed in [6].

The contribution of this thesis is that the IRP theory, originally developed for three-phase implementation, is adapted for single phase; in addition, the IRP (αβ) theory control scheme is implemented and compared to a functioning EMS with a root mean square (RMS) control method [19]. A detailed analysis is conducted on the feasibility and implementation of either control method. The viability of both methods is validated by simulations and comparison of the two methods conducted in a MATLAB and SIMULINK environment.

The generic EMS, illustrated in Figure 4, and the detailed specifics of the model subsystems are discussed in Chapter II. The root-mean square (RMS) and IRP (αβ) theory required for reactive power insertion and unity power factor are detailed in Chapter III. SIMULINK testing and an analysis of simulated results are discussed in Chapter IV. Lastly, conclusions and future work are discussed in Chapter V.

II. ENERGY MANAGEMENT SYSTEM MODEL AND DESIGN

A. SYSTEM OVERVIEW

The Energy Management System (EMS), introduced in the previous chapter, is now discussed in further detail. Utilizing an EMS to maintain system stability, controllability, and provide active and reactive power control is a common engineering practice used in many grid control applications [20], [21]. From Figure 4 we see that the EMS, as the name implies, manages energy storage, grid interface, and critical/non-critical loads. An EMS that can be used to provide power to both critical and non-critical loads either from the AC grid, the battery, or in a load-sharing scenario is illustrated in Figure 4. Load-sharing allows for peak shaving during periods of high power demand, minimizing cost to the customer. In addition to managing loads, the EMS can be used to integrate renewable power sources such as wind turbines and solar power with existing diesel generators. This allows a military microgrid deployment to assist in abating the logistical difficulties required for typical diesel generators and their reliance on diesel fuel. The EMS architecture and integrated systems used to accomplish the grid applications are discussed in this chapter.

1. EMS Architecture

The EMS, shown in Figure 4, is a power electronic based system. It is coupled to the main grid and includes a single-phase Voltage Source Inverter (VSI) with an inductor-capacitor (LC) filter. The LC filter provides the required sinusoidal voltage for the AC load by filtering out high-order harmonics from the switches. The EMS also consists of a buck and boost converter to assist in either charging the internal battery when in AC grid mode or supplying power to the load when in islanding mode.

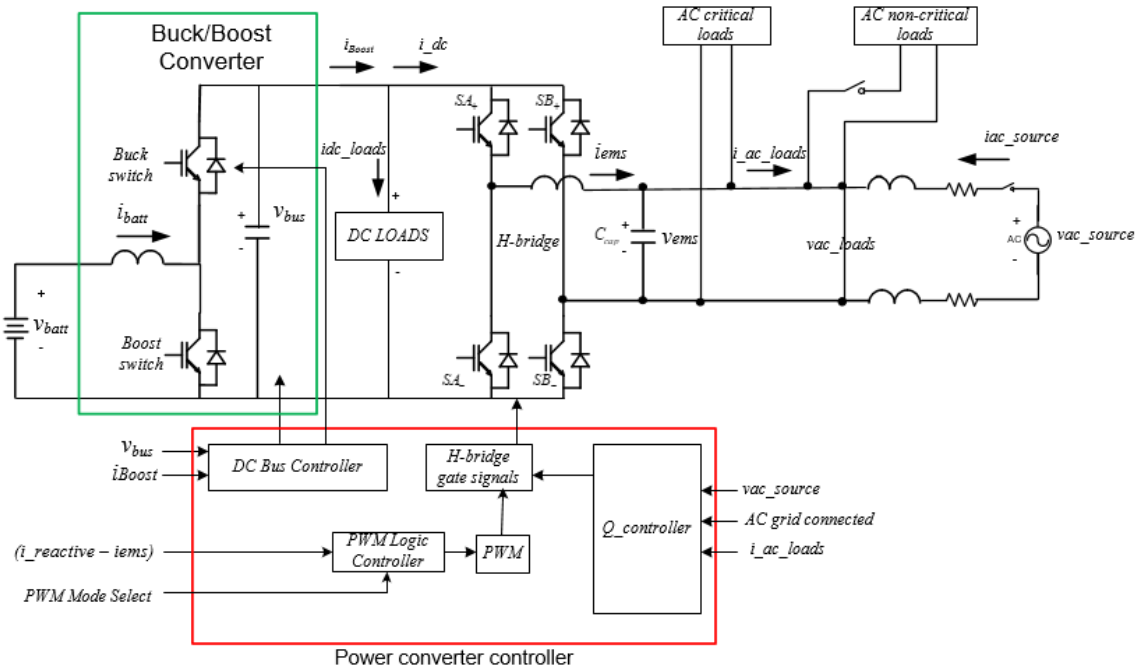

Figure 4. EMS Architecture. Source [22].

This model emulates combatant ship/submarine design by connecting critical loads directly to the AC grid, providing constant power. Non-critical loads are connected in parallel to the AC grid and can be disconnected as the situation dictates. In the event that the AC grid does not provide power reliably due to reasons such as extreme weather, cyber-attack, or maintenance, the EMS can be disconnected from the grid and operate in islanding mode. When transitioned and operating in islanding mode, no interruption of power to critical loads occurs because power is supplied from the internal battery.

2. EMS Operation

The power converter-controller module contains three subsystems that provide inputs to the single-phase VSI and the DC bus. The *Q_controller* subsystem receives inputs from both source voltage and current and verifies the EMS is in grid-connected mode. The *Q_controller* then provides an output reactive insertion current signal to the H-bridge gate signal module. The *PWM* block receives inputs form the difference of reactive and EMS current along with *PWM* mode, which can be either unipolar or bipolar, discussed later in this section. The generated PWM reference output is sent as an

input to the H-bridge gate signals subsystem and drives the VSI Insulated Gate Bipolar Transistors (IGBTs) to meet the AC load voltage and current demands. Lastly, the DC bus controller, depending on the operating mode of the EMS (islanding or grid-connected), directs current either to assist in supplying the load or to charge the internal battery.

B. MODEL AND DESIGN

The model illustrated in Figure 5 was developed and evaluated using MATLAB and SIMULINK. The individual building blocks of this model and the ways they contribute to the system as a whole are discussed in this section.

1. EMS Model

The heart of the microgrid is encapsulated in the EMS. Rather than using a block diagram approach, with the tools available in SIMULINK, the EMS is built using individual components and well-known electrical engineering theories and calculations. Kirchhoff's voltage and current laws are used to determine expected output voltage/current for different EMS modes of operation.

2. Integrated System

The integrated block diagram system is illustrated in Figure 5. Observe that all the major components in the simplified diagram seen in Figure 4 (red box) are present in the block diagram of Figure 5. Two major inputs include the AC grid (*AC grid on*) and the mode of operation for the switching network (*PWM_mode*). The AC grid on is activated by inserting a step load change, and the *PWM_mode* (unipolar/bipolar) can be changed in the MATLAB initial conditions based on the desired mode of operation. The Proportional Integral (PI) controller compares the reference voltage (*vo_ref*) and the estimated voltage (*vo_est*) to provide the proper duty cycle input to the pulse-width modulation (PWM) block. The LC filter/inductor-resistor (LR) load system takes the switching mode, the bus voltage (*v_bus*), the current drawn by the load (*i_ac_loads*), and the source current (*i_ac_source*) to provide the estimated voltage (*vo_est*). In addition, the EMS current (*i_ems*) can be used as supplemental current in the event the AC grid does not provide

adequate power. Lastly, the reactive current control, the focus of this thesis, compares the voltage and current signals provided by the AC grid and provides the requisite reactive current compensation to ensure a unity pf.

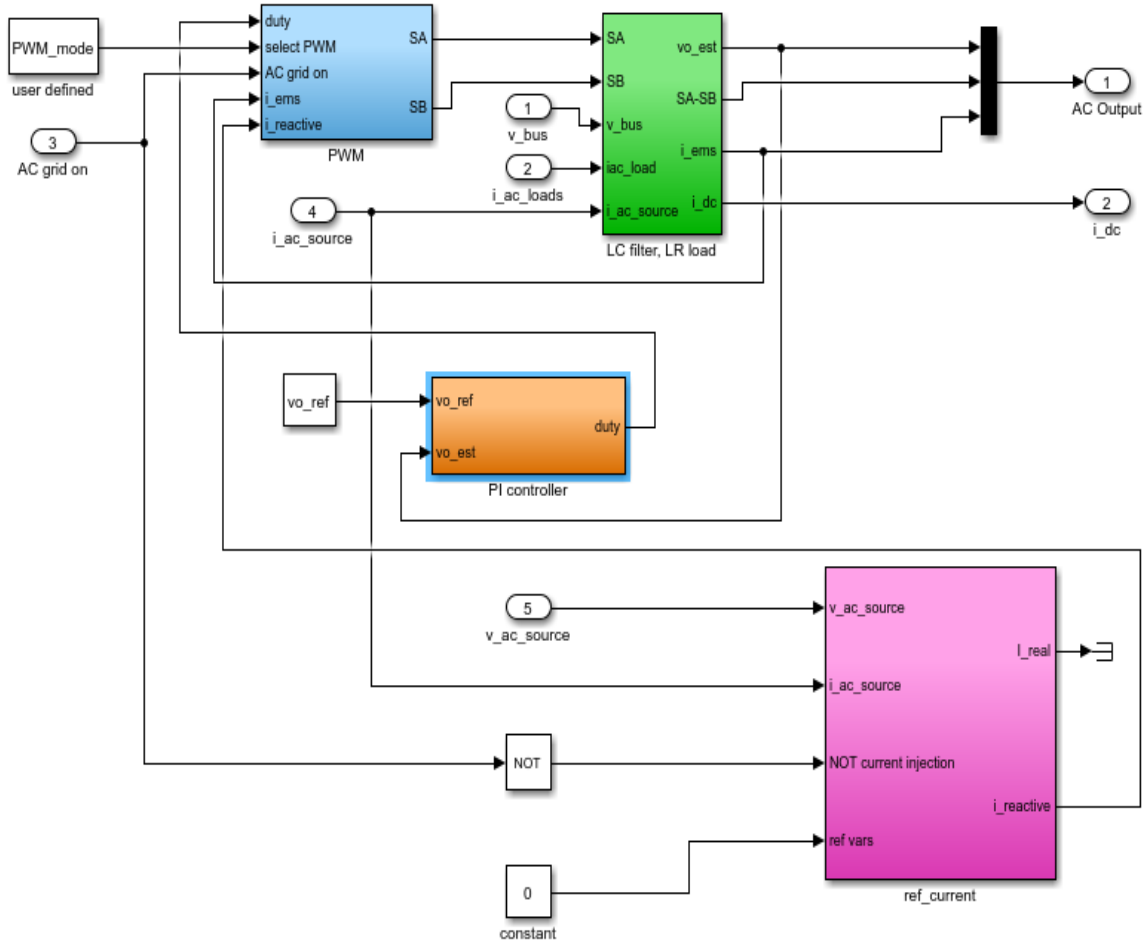

Figure 5. EMS Integrated System

3. PWM System

The PWM circuit illustrated in Figure 6 is enabled with a step load change that can be manipulated in the initial conditions file for the SIMULINK model.

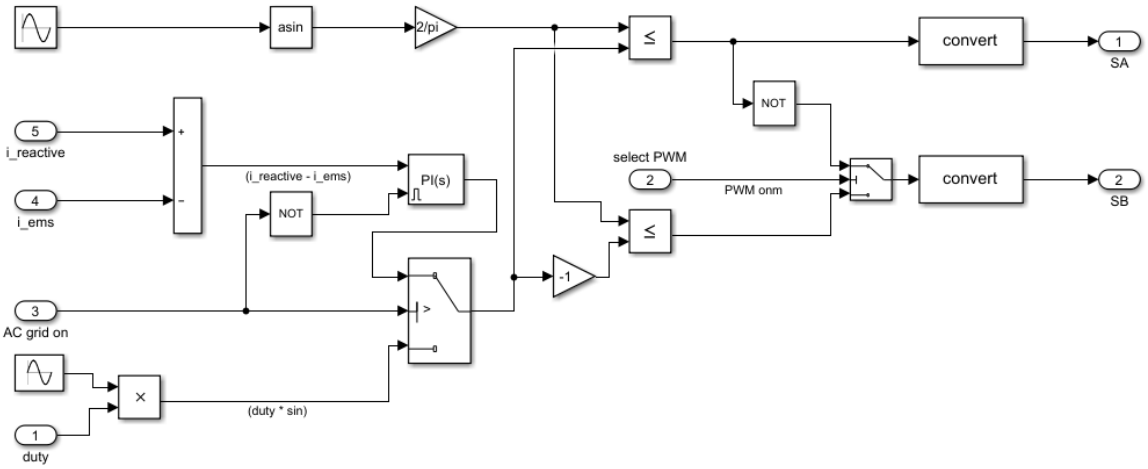

Figure 6. PWM System

Once enabled, the EMS current (*i_ems*) is compared with *i_reactive* current, generated from the grid voltage and current. The final output is sent to a PI controller. A verification that the AC grid is conducted and the switching signals *SA* and *SB* for the VSI IGBTs are generated based on a desired input switching frequency. A user-defined input in the initial condition file allows the mode of operation to be changed from unipolar to bipolar. Unipolar and bipolar PWM for the H-bridge inverter depicted in Figure 7 are implemented as follows:

- PWM bipolar: the pair of switches (*SA*+, *SB*-) and (*SA*-, *SB*+) are controlled on or off simultaneously. One of the two pairs is always on.
- PWM unipolar: switches in each inverter leg are controlled independently.

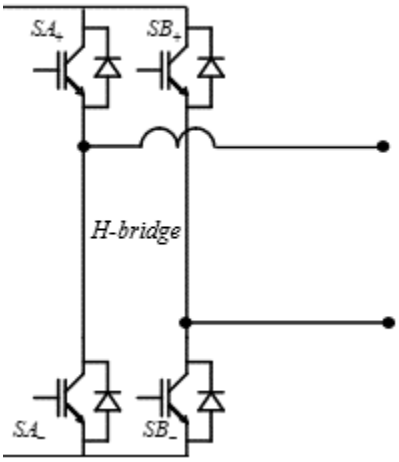

Figure 7. H-Bridge Inverter Switching Scheme

The EMS model is built for both modes of operation for completeness of the model. In all testing the switching frequency of the switches was the same and set by the user in the MATLAB initial conditions input. All testing was done in unipolar operation due to the advantages outlined in N. Mohan et al. [23]. These advantages include better output voltage waveform, reduced ripple voltage, and better frequency response.

4. PWM Filter

The second component of the EMS integrated system is the PWM filter. The PWM filter is modeled from the voltage and currents that are needed to supply the load from the EMS. Recall from Figure 4, partially shown in Figure 8, that current from the EMS, AC source, and the load are required for the derivation of the EMS voltage.

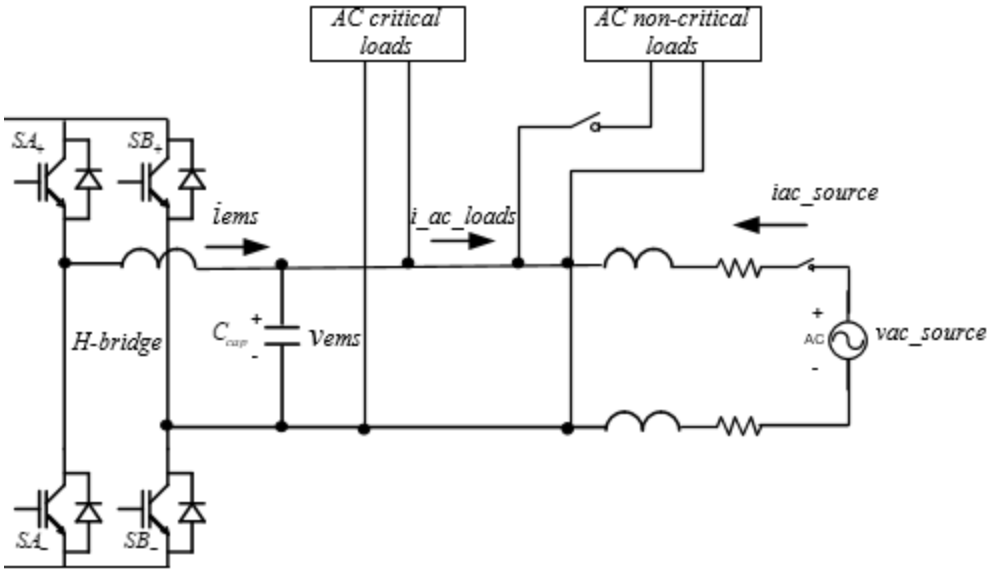

Figure 8. Partial EMS Architecture

The mathematical model derived from Kirchoff's current law and Laplace domain is

$$C_{cap} s v_{ems} = i_{ems} + i_{ac\_source} + i_{\_ac\_load} . \quad (1)$$

This equation is an integral part of the PWM filter shown in Figure 9. In (1), the source current and load current are summed with the EMS current.

In order to derive the EMS current, the switching states (*SA/SB*) which are derived from the PWM system are subtracted and multiplied with the bus voltage (*v_bus*). This calculation provides the desired AC voltage needed for integration to produce the EMS current (*i_ems*). Estimated voltage (*v_est*) is then calculated using (1) by dividing the summation of all the currents by a known capacitance and integrating to derive the final value.

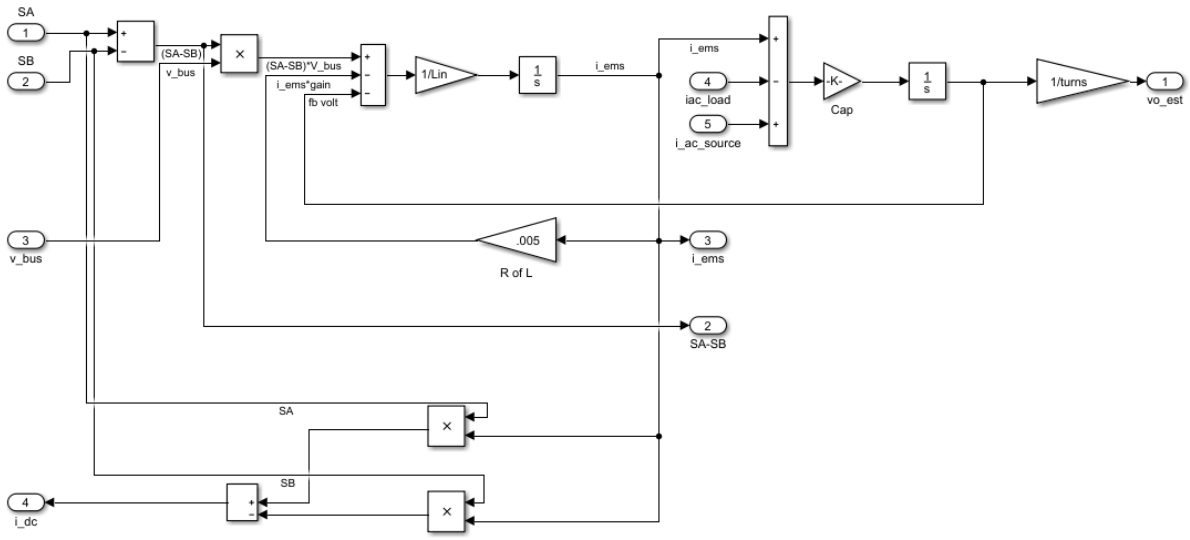

Figure 9. PWM Filter

A system overview of the EMS model was covered in this chapter. The model is used to control the microgrid reactive power in the next chapter. Reactive current control was briefly discussed in this chapter and is further discussed in Chapter IV.

III. REACTIVE CURRENT CONTROL

The model and design of the EMS subsystems were discussed in Chapter III with the exception of the reactive current control. The last major subsystem, and the focus of this thesis, is the derivation of reactive current using two control schemes. As noted previously, the EMS model allows for two methods of reactive current control, and either method can be implemented in the MATLAB initial conditions.

A. REACTIVE POWER COMPENSATION

In review, a main objective of the EMS is to show how the Q_control subsystem can inject reactive power to the grid. This can be done with either the IRP (αβ) theory or the RMS control scheme. Reactive power demand by the AC load can be corrected to achieve unity pf with either control scheme when in AC grid-connected mode. Despite the method chosen, the following is a simplified phasor notation functional description of the EMS unity power factor correction.

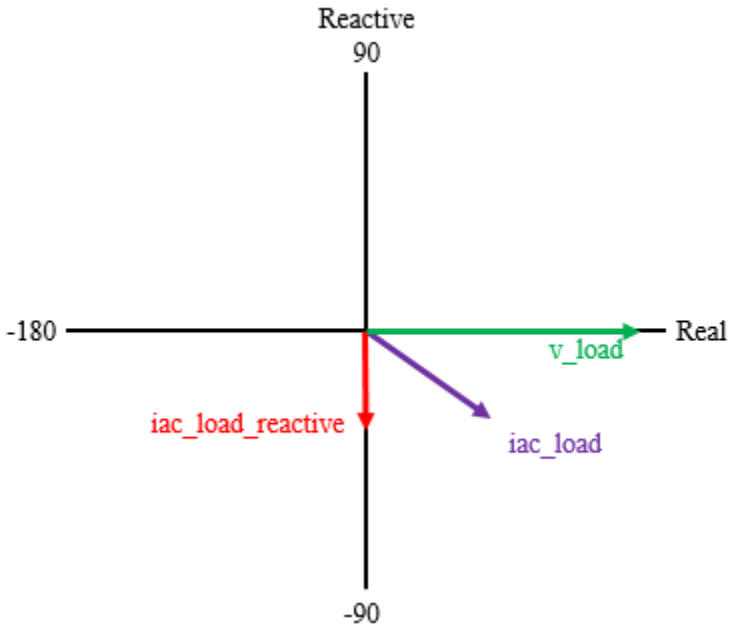

Figure 10. Phasor Diagram for AC Load Voltage and Current

A complex-number plane in which the X-axis represents the real axis and the Y-axis represents the imaginary axis is shown in Figure 10. Current and voltage are expressed in phasor notation with a magnitude and phase angle. All scenarios examined in this thesis include an inductive load causing the current to lag the voltage. From Figure 10, we see what a phasor diagram representing the load current prior to EMS current (*i_ems*) correction being applied looks like. The load current phasor (*iac_load*) has a real and imaginary component (*iac_load real* and *iac_load_reactive*).

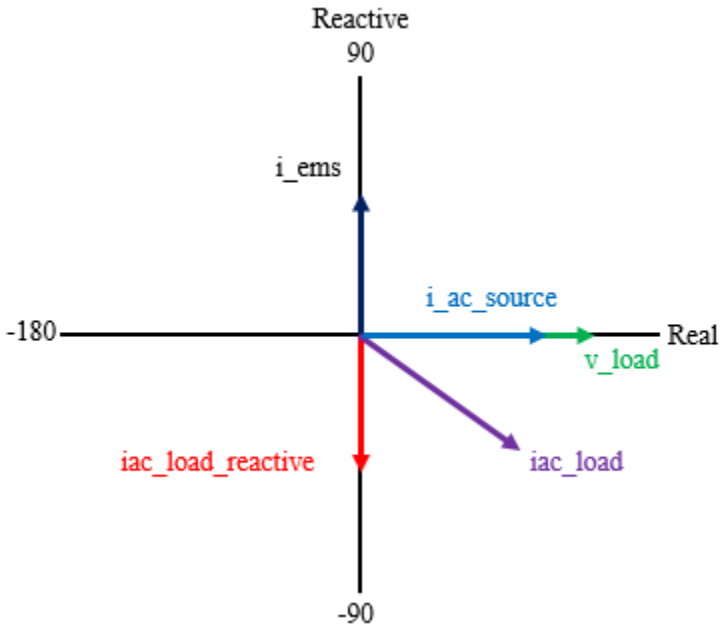

Figure 11. Phasor Diagram with *i_ems* Current Activated

When the EMS is in grid-connected mode, the *Q_control* subsystem compensates for the inductive AC load by providing current with a reactive component (*i_ems*) equal in magnitude and opposite that of the AC load. Once steady state is reached, source voltage and current (*v_source* and *i_source*) are in phase and have a unity pf as depicted in Figure 11.

B. RMS CONTROL

The RMS method is discussed first, and a SIMULINK model is illustrated in Figure 12.

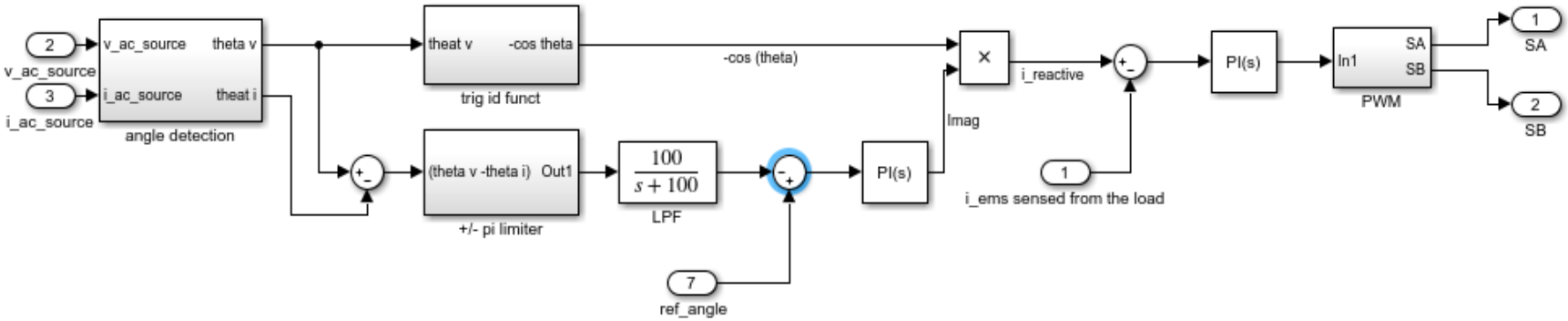

Figure 12. RMS Reactive Current Control Scheme

While operating in AC grid-connected mode, the grid voltage and current (*v_ac_source* and *i_ac_source*) are provided as inputs to the subsystem in order to determine the phase of each sinusoidal voltage and current input. The phase angle difference of the source voltage and current $\left(\phi_v - \phi_i\right)$ is determined and sent through a low pass filter. The new filtered signal is subtracted from a reference angle $\left(\mathit{filtered\_signal} - \mathit{ref\_angle}\right)$ and sent to a PI controller, which outputs the imaginary component needed for *i_reactive*. In the parallel path, the source voltage input phase (*theta v*) is passed to a trigonometry identity function prior to being multiplied with the amplitude Imag $\left(\mathrm{Imag} \times \left(-\cos\left(\mathit{theta}\right)\right)\right)$. The final output *i_reactive* provides the imaginary component that the EMS needs to produce unity pf. The RMS SIMULINK model is shown in Figure 13.

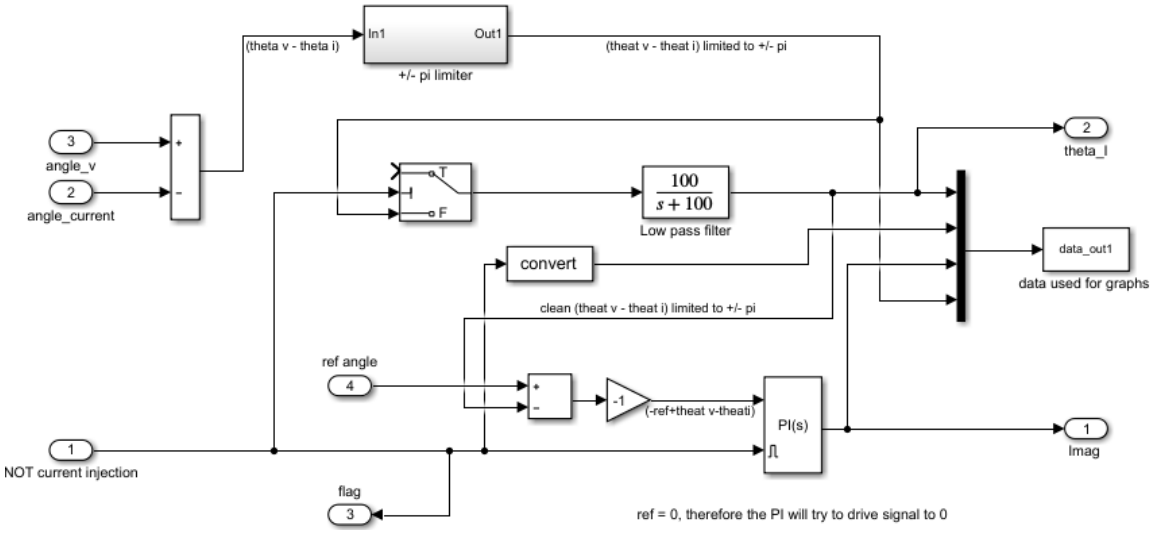

Figure 13. RMS Reactive Current Control SIMULINK Model

C. INSTANTANEOUS REACTIVE POWER (IRP) THEORY CONTROL

The second control method for reactive current utilizes the IRP theory in a reference frame with two orthogonal axes (αβ) [24]. This control scheme is normally applied to three-

phase systems but is effective in single-phase systems as well. The transition of application from three-phase to single-phase systems applies to the two orthogonal axes α and β. Single-phase systems only require one variable; therefore, a fictitious axis must be created.

The IRP (αβ) theory inverter control scheme, illustrated in Figure 14, is used to generate the reactive current compensation in a single-phase system [24]. Source voltage and current are provided as inputs as is the case for the RMS control scheme. The IRP (αβ) control scheme provides two output currents in which the fictitious current is discarded and the reactive current is used to compensate for the inductive load, as was the case for the RMS control scheme.

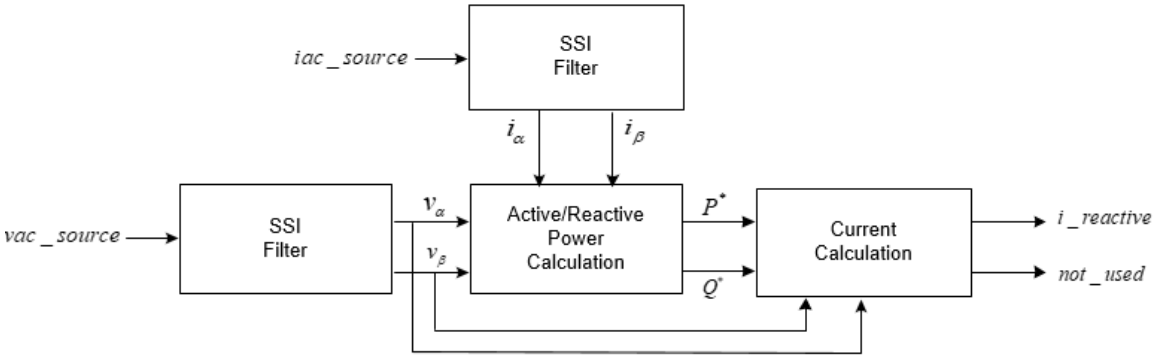

Figure 14. IRP αβ Control Scheme. Adapted from [23].

In addition to the single-phase adaptation, Bojoi et al. incorporates the use of a sinusoidal-signal integrator (SSI) [25], [26]. The SSI is used to derive the transfer functions that are necessary for the desired reactive control output. The IRP (αβ) SIMULINK model is illustrated in Figure 15.

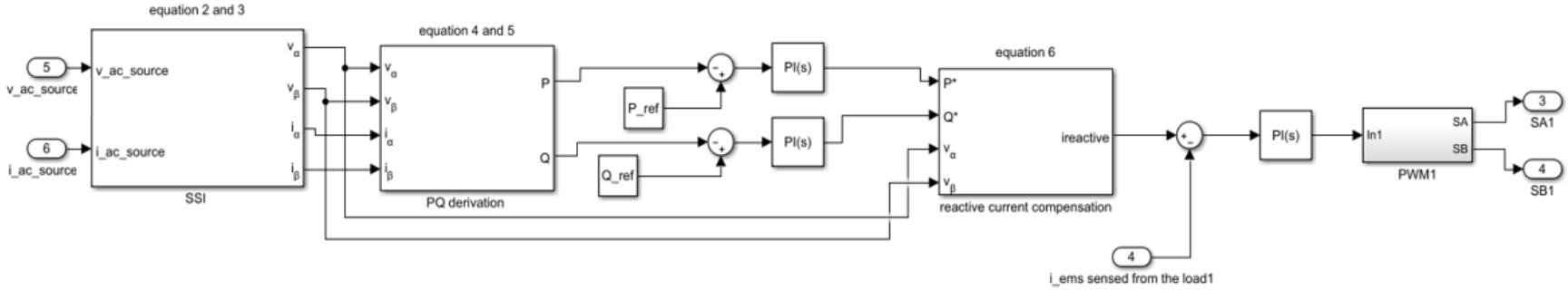

Figure 15. IRP (αβ) Control Scheme

The model seen in Figure 15 takes the sinusoidal source voltage and current inputs and applies the SSI model transfer functions (2) and (3), respectively, to obtain the voltage and current αβ components

$$H_1(s) = \frac{i_\alpha(s)}{i_{\_ac\_source}(s)} = \frac{2k_A \times s}{s^2 + 2k_A \times s + \omega_0^2} = \frac{v_\alpha(s)}{v_{\_ac\_source}(s)}, \tag{2}$$

$$H_2(s) = \frac{i_\beta(s)}{i_{\_ac\_source}(s)} = \frac{2k_A \times \omega_0}{s^2 + 2k_A \times s + \omega_0^2} = \frac{v_\beta(s)}{v_{\_ac\_source}(s)}, \tag{3}$$

where k_A is the gain constant and ω_0 is the angular frequency. The orthogonal output voltages and currents are then used by *the PQ derivation* block, as seen in Figure 15. The *PQ derivation* block uses (4) and (5) to calculate P and Q:

$$Q = i_\alpha v_\beta - i_\beta v_\alpha, \tag{4}$$

and

$$P = i_\alpha v_\beta + i_\beta v_\alpha. \tag{5}$$

P and Q are compared to their reference values (*P_ref* and *Q_ref*), and the resulting error goes through a PI controller to generate $P^*$and Q^*. The P^*, Q^*, and orthogonal voltage components are used to generate the reference current required to determine the amount of reactive current insertion needed for unity power factor:

$$\begin{bmatrix} i_\alpha^* \\ i_\beta^* \end{bmatrix} = \frac{1}{v_\alpha^2 + v_\beta^2} \begin{bmatrix} v_\alpha & v_\beta \\ v_\beta & -v_\alpha \end{bmatrix} \times \begin{bmatrix} P^* \\ Q^* \end{bmatrix}. \tag{6}$$

A brief summary of reactive power and the importance of a unity pf was recapped at the start of this chapter. The focus was a complete understanding of the RMS and IRP αβ control schemes. A detailed one-line schematic integrated both the signal flow and the calculations required for both schemes to produce a unity pf. Simulation and testing of both schemes are the focus of the next chapter.

THIS PAGE INTENTIONALLY LEFT BLANK

IV. SIMULATION AND TESTING

The two EMS reactive current control schemes were discussed in Chapter IV, and in Chapter V, we focus on simulation and testing. All testing was conducted in MATLAB and SIMULINK, and ideal components were used for all building blocks.

A. RMS AND IRP CONTROL SCHEME UNITY PF TESTING INITIAL CONDITIONS

The simplified circuit design used for the unity pf test is illustrated in Figure 16. Test conditions require the EMS to be in grid-connected mode and have a user-defined load.

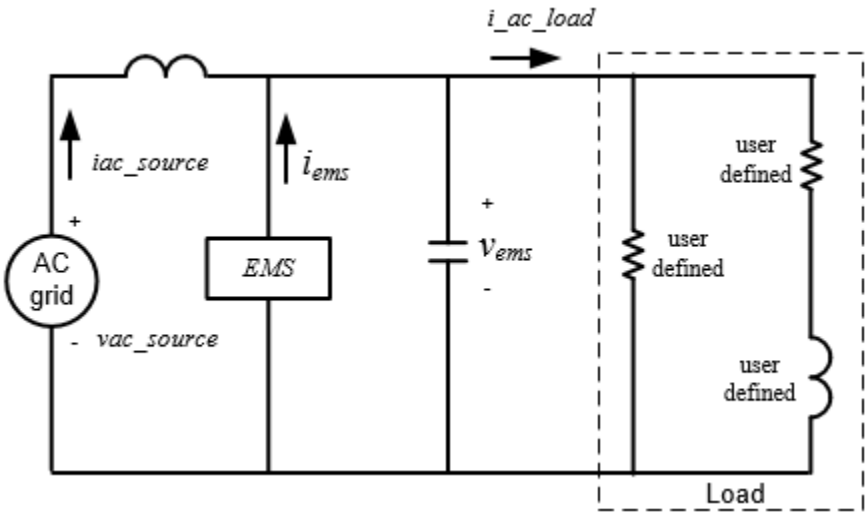

Figure 16. Simplified Circuit Design for EMS Testing

The MATLAB script allows the user to input values for the load or the MATLAB script can create a load based on a desired initial pf. The load design used in SIMULINK for testing can be seen in Figure 17.

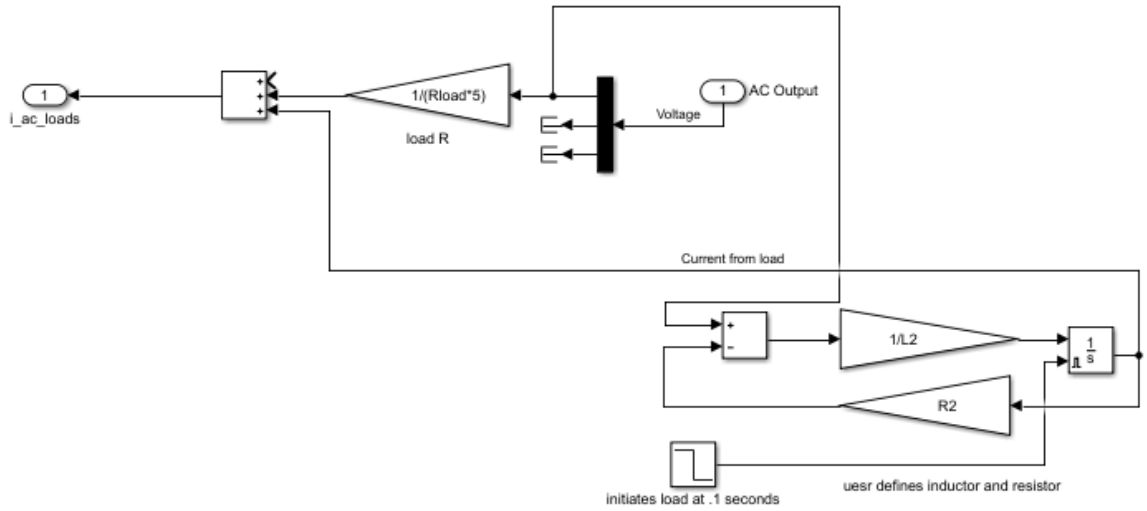

Figure 17. EMS AC Load Model

B. RMS AND IRP CONTROL SCHEME UNITY PF TESTING

The first test conducted on the model is to verify the validity of both control schemes when the pf needs to be compensated. The goal is to evaluate both methods of reactive current compensation to see if one method was more desirable for implementation into the EMS model. The test parameters that were chosen based on their suboptimal values of pf are seen in Table 1.

Table 1. Component Values Used for the Unity pf Test

Component Values	**Test 1**	**Test 2**
Resistor	4.10 Ω	7.71 Ω
Inductor	30 mH	24 mH
PF before/after	0.34/1	0.64/1
Impedance (Z)	4.10+j11.28	7.71+j9.19
Figure(s)	18-20	21-23

C. RMS AND IRP CONTROL SCHEME UNITY PF TESTING RESULTS

In the RMS and IRP (αβ) control scheme scenarios, a step-load change is initiated at 0.1 to simulate both EMS AC grid-connected mode and a series resistive-inductive load as seen in Figure 16. Immediately, AC grid current and AC grid voltage supply the load. Due to the inductive load for both scenarios listed in Table 1, current lags the voltage.

Test 1 observation results for the RMS control unity pf correction are shown in Figure 18. AC grid voltage and current are plotted versus time in the upper graph, and AC grid voltage and EMS current are plotted versus time in the lower graph.

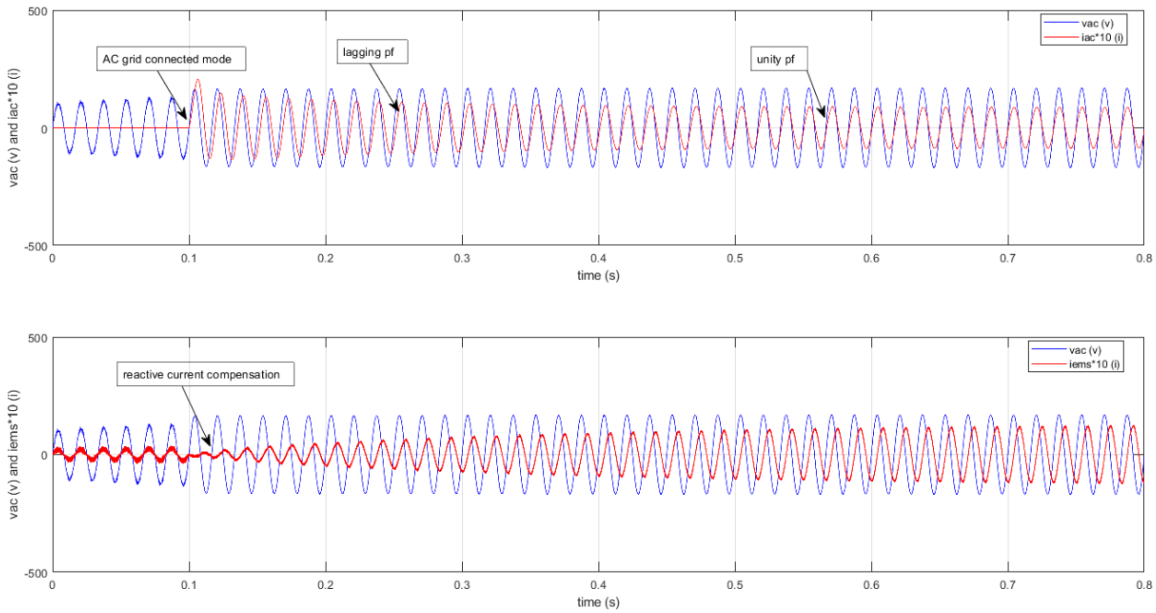

Figure 18. Test 1 RMS Control Unity pf

Test 1 observation results for the IRP (αβ) control unity pf test are shown in Figure 19. As in Figure 18, AC grid voltage and current are plotted versus time in the upper graph, and AC grid voltage and EMS current are plotted vs time in the lower graph.

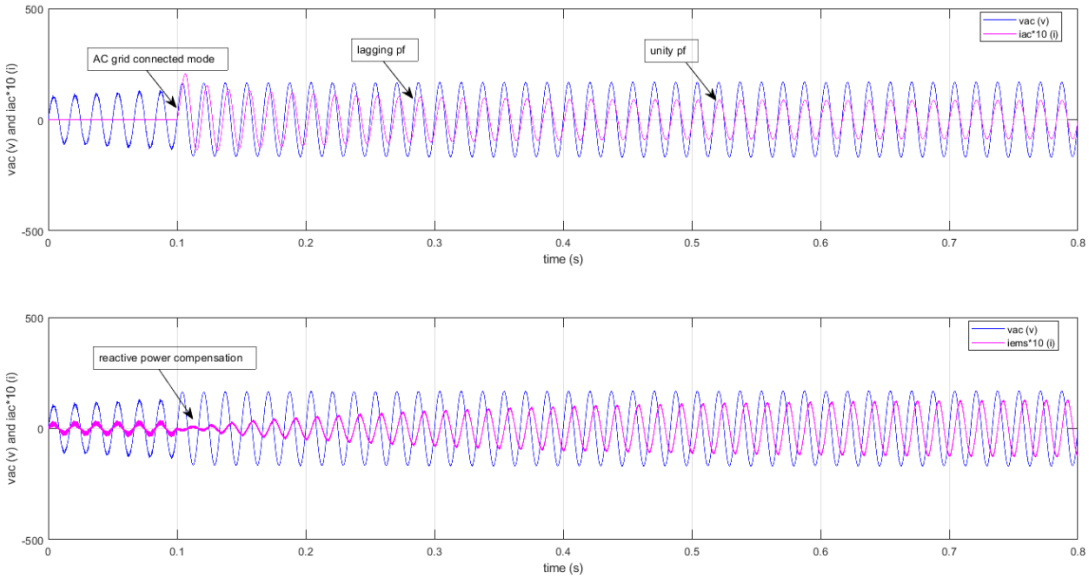

Figure 19. Test 1 IRP (αβ) Control Unity pf

The Test 1 calculated P-Q results for the unity pf test are shown in Figure 20. Real power (P) and reactive power (Q) are shown in the upper and lower graphs, respectively, for both control schemes.

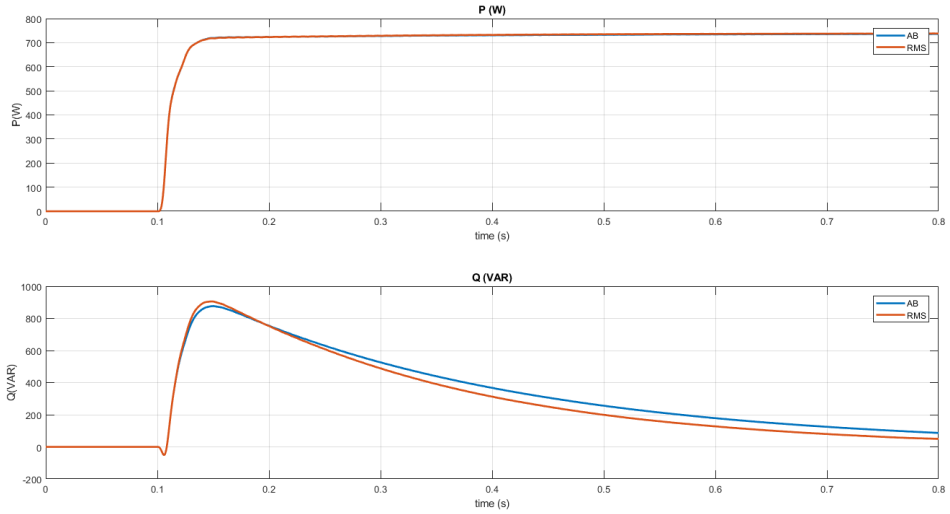

Figure 20. Test 1 P-Q Calculations Unity pf

Test 2 observation results for the RMS control unity pf correction are shown in Figure 21. AC grid voltage and current are plotted versus time in the upper graph, and AC grid voltage and EMS current are plotted versus time in the lower graph.

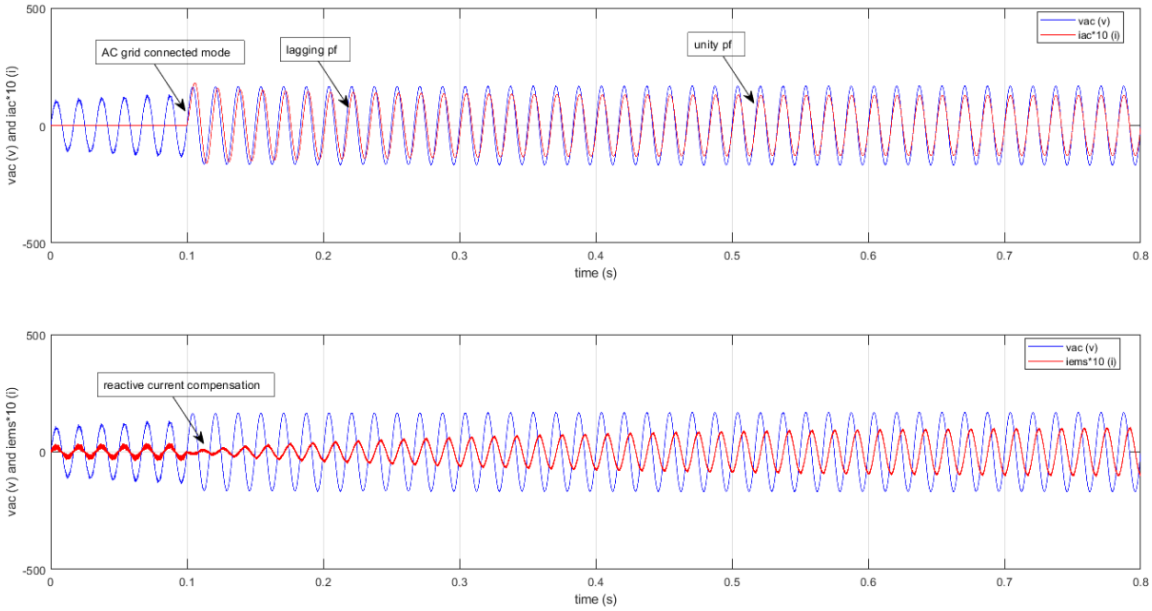

Figure 21. Test 2 RMS Control Unity pf

Test 2 observation results for the IRP (αβ) control unity pf test are shown in Figure 22. As in Figure 21, AC grid voltage and current are plotted versus time in the upper graph, and AC grid voltage and EMS current are plotted versus time in the lower graph.

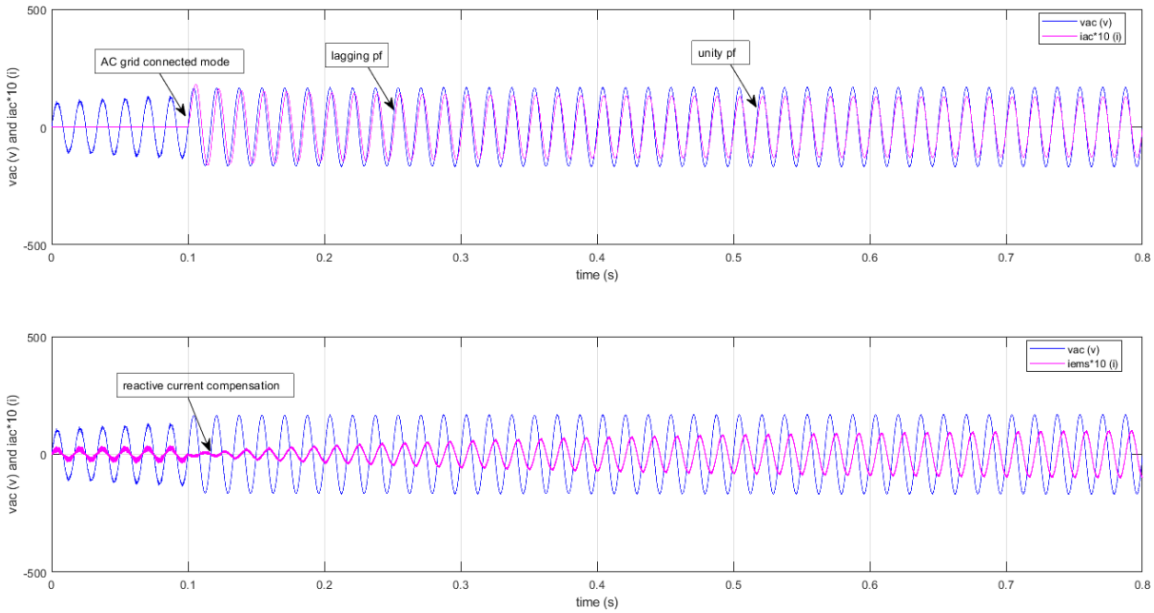

Figure 22. Test 2 IRP (αβ) Control Unity pf

The Test 2 calculated P-Q results for the unity pf test are shown in Figure 23. Real power (P) and reactive power (Q) are shown in the upper and lower graphs, respectively, for both control schemes as was done in Figure 20 for Test 1.

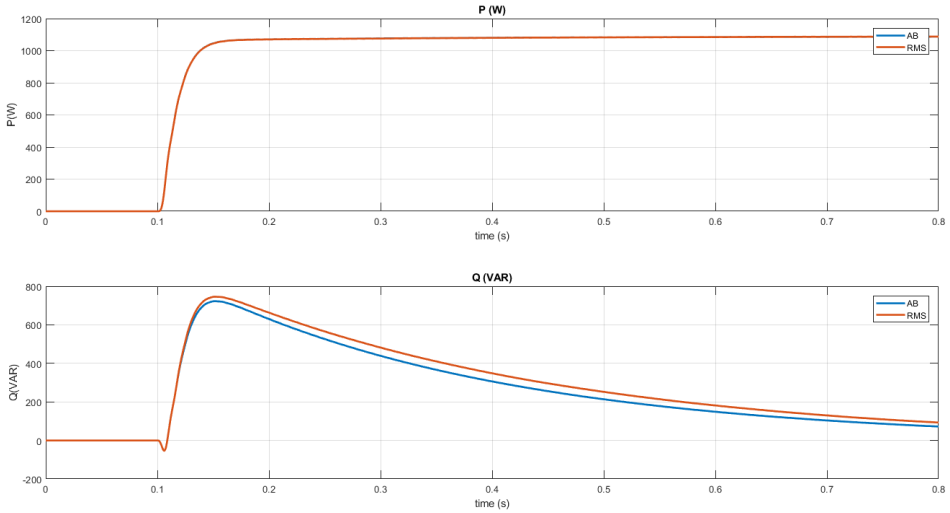

Figure 23. Test 2 P-Q Calculations Unity pf

We see in the upper graphs of Figures 18-19 and Figures 21-22 that both the RMS and IRP αβ control schemes correct for an initial suboptimal pf to unity pf with minimal difference. At time 0.1 s the lagging pf is visually observable, and within approximately 0.4 s to 0.5 s unity pf is achieved. We see in the lower graphs in Figures 18-19 and Figures 21-22 that for any given load the EMS current compensates to achieve unity pf.

In both the upper graphs of Figures 20 and 23, we see that real power is supplied to the load at 0.1 s with no distortion or abnormalities. We see in the lower graphs of these same figures that reactive power approaches zero, unity pf, for both control schemes. Additionally, the RMS control scheme is shown to have a slight advantage over the IRP (αβ) control scheme. Despite the minimal advantage of the RMS scheme, both methods were found to be effective overall and equivalent.

D. RMS AND IRP CONTROL SCHEME TRANSIENT TESTING INITIAL CONDITIONS

In addition to testing of both control schemes for unity pf correction, the system was also tested for inductive transients. The schematic for transient testing is illustrated in Figure 24.

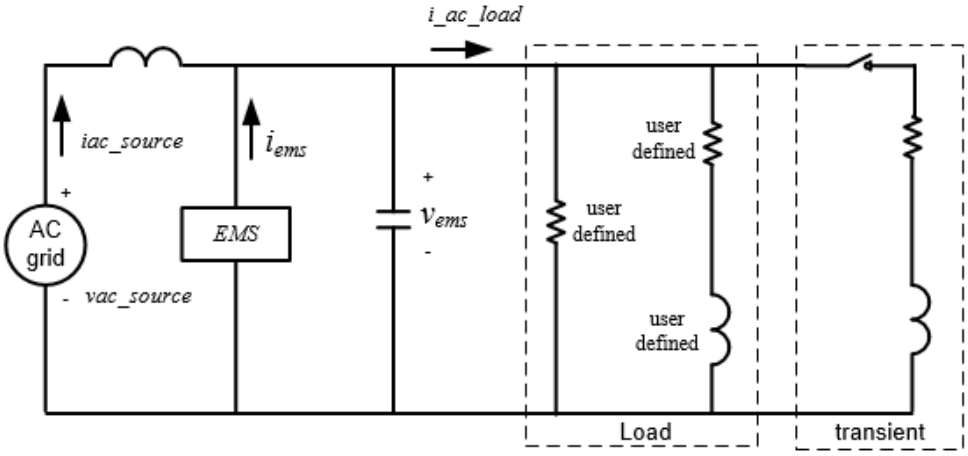

Figure 24. Simplified Circuit Design for Transient Testing

The MATLAB script user input is the same as for the unity pf test with the exception of the two new components that simulate the transient. The SIMULINK model used for testing is illustrated in Figure 25.

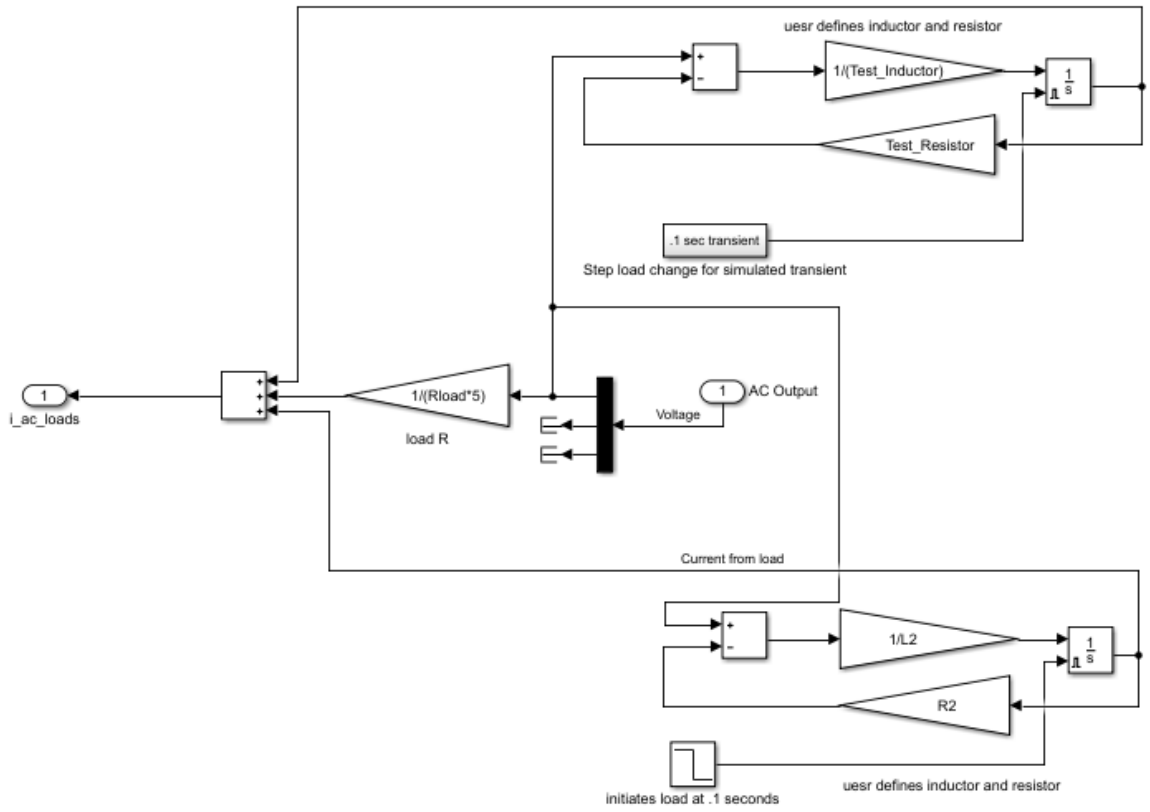

Figure 25. EMS AC Load Model with Transient

E. RMS AND IRP CONTROL SCHEME TRANSIENT TESTING

Once testing was complete for the unity pf correction, additional testing was developed to ensure robustness for a simulated transient environment. Transient testing uses the same initial conditions used in Test 1 along with the new values for the simulated transient load. The intention of this test is to evaluate both methods of reactive current compensation prior to and throughout the transient. Observations are made on the ability to recover from the transient and still provide unity pf correction. All values used for the transient test are listed in Table 2.

Table 2. Component Values Used for the Transient Test

Component Values	**Test 1**	**Test 2**
Resistor	4.10 Ω	4.10 Ω
Inductor	30 mH	30 mH
pf before/after	0.34/1	0.34/1
Impedance (Z)	4.10+j11.28	4.10+j11.28
Transient Resistor	1 Ω	4.10 Ω
Transient Inductor	25 mH	30 mH

F. RMS AND IRP CONTROL SCHEME TRANSIENT TESTING RESULTS

As in the RMS and IRP (αβ) control scheme unity pf test, a step-load change was initiated at 0.1 s to simulate both EMS AC grid-connected mode and a series resistive-inductive load as seen in Figure 25. The test also includes a 0.5 s delay upon which the switch seen in Figure 25 shuts. The switch adds the transient load to be included as part of the circuit until 0.1 s later when the switch reopens. This switch action simulates a 0.1 s transient while in AC grid-connected mode with a series connected resistive-inductive load.

Test 1 observation results for the RMS control transient test are shown in Figure 26. AC grid voltage and current are plotted versus time in the upper graph, and AC grid voltage and EMS current are plotted versus time in the lower graph.

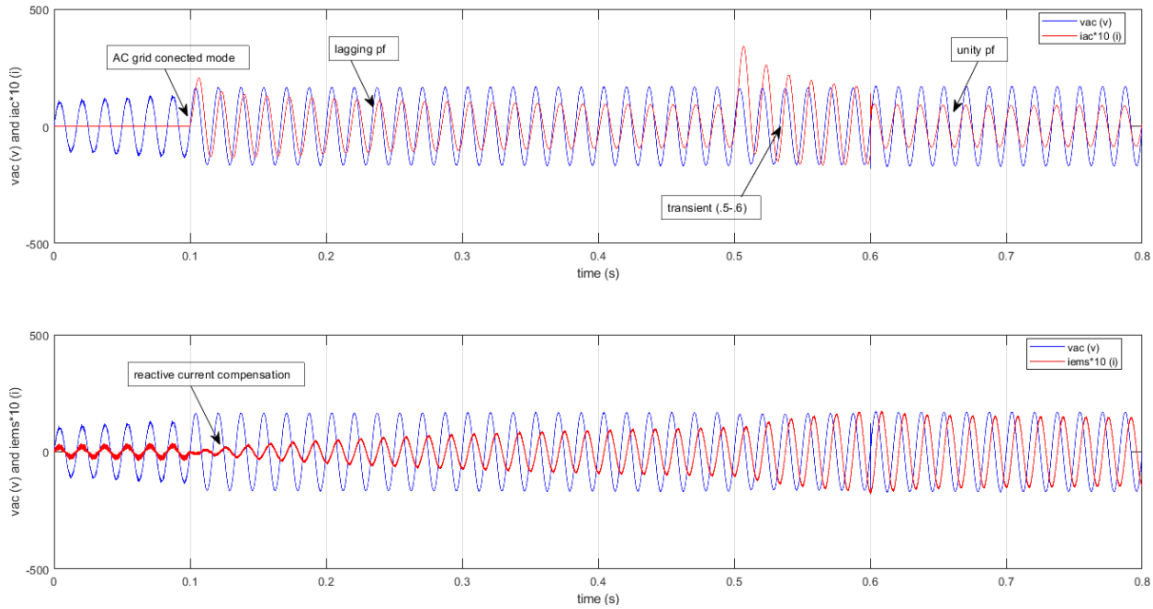

Figure 26. Test 1 RMS Control Transient

Test 1 observation results for the IRP (αβ) control transient test are shown in Figure 27. As in Figure 26, AC grid voltage and current are plotted versus time in the upper graph, and AC grid voltage and EMS current are plotted versus time in the lower graph.

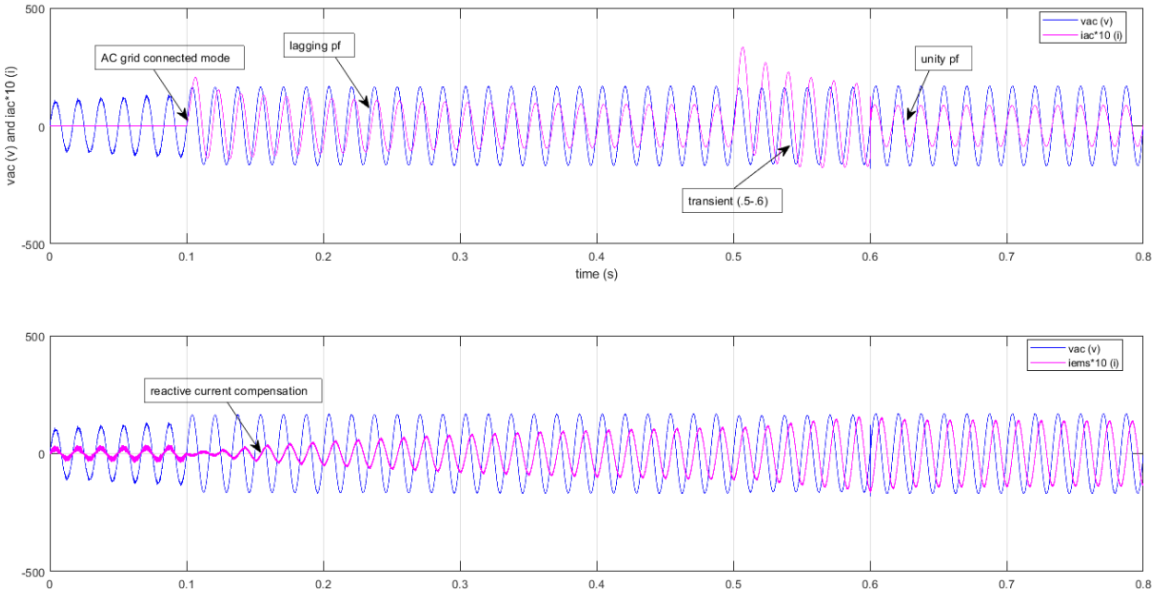

Figure 27. Test 1 IRP (αβ) Control Transient

The Test 1 calculated P-Q results for the transient test are shown in Figure 28. Real power (P) and reactive power (Q) are shown in the upper and lower graphs, respectively, for both control schemes.

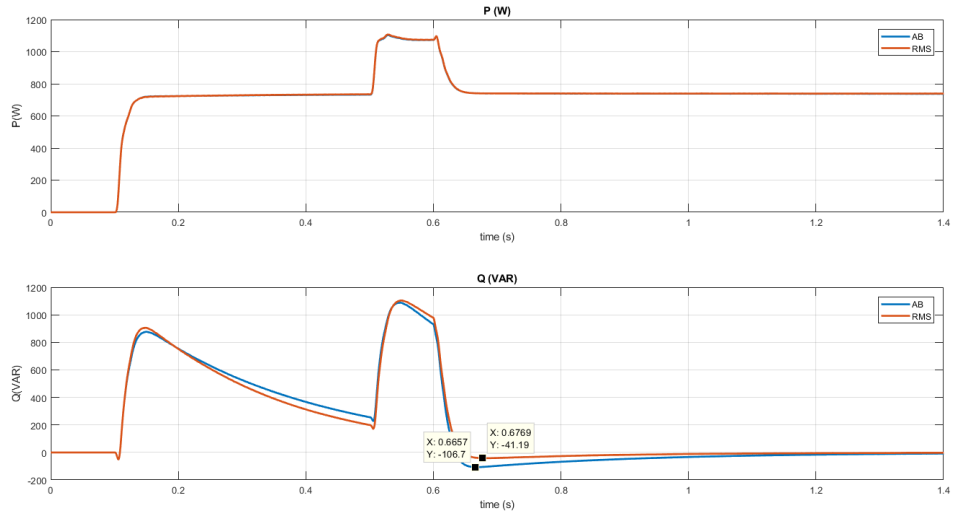

Figure 28. Test 1 P-Q Transient Calculations

Test 2 observation results for the RMS control transient test are shown in Figure 29. AC grid voltage and current are plotted versus time in the upper graph, and AC grid voltage and EMS current are plotted versus time in the lower graph.

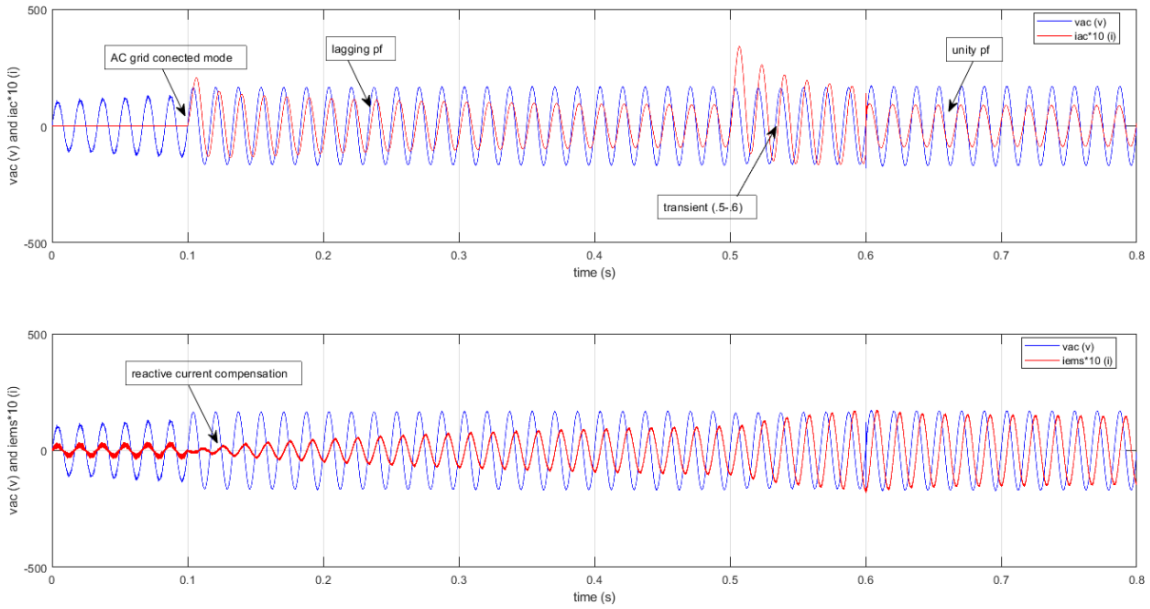

Figure 29. Test 2 RMS Control Transient

Test 2 observation results for the IRP (αβ) control transient test are shown in Figure 30. As in Figure 29, AC grid voltage and current are plotted versus time in the upper graph, and AC grid voltage and EMS current are plotted versus time in the lower graph.

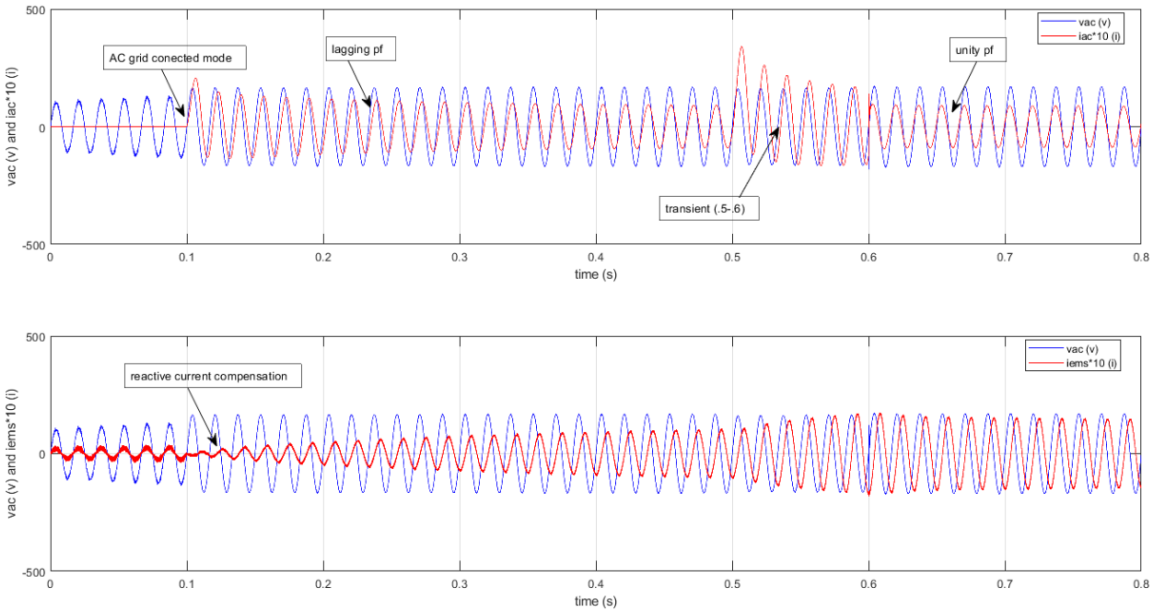

Figure 30. Test 2 IRP (αβ) Control Transient

The Test 2 calculated P-Q results for the transient test are shown in Figure 31. Real power (P) and reactive power (Q) are shown in the upper and lower graphs, respectively, for both control schemes as was done in Figure 28 for Test 1.

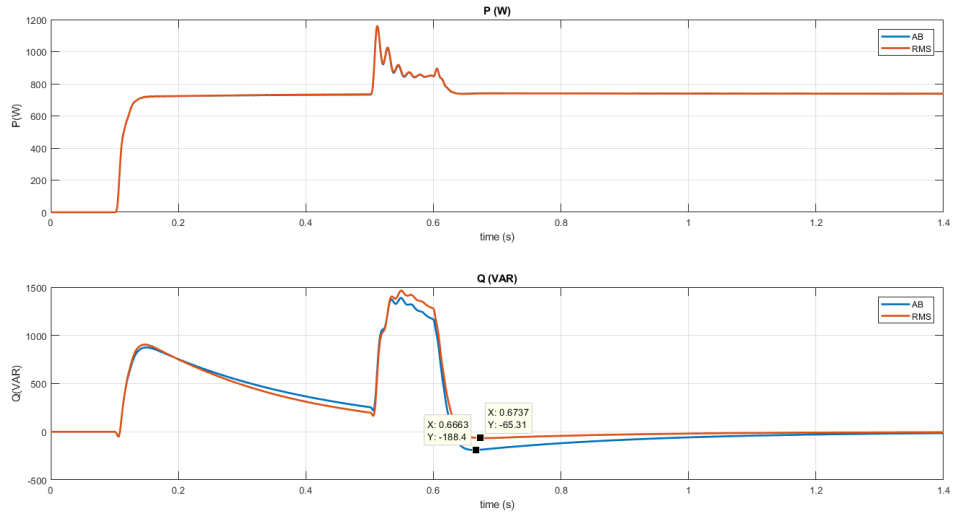

Figure 31. Test 2 P-Q Transient Calculations

As illustrated in Figures 26–31, the EMS provides reactive compensation and functions identically to the unity pf test until the transient is applied at 0.5 s. The transient is visible with a spike and erratic behavior in real and reactive power as illustrated in Figures 28 and 31. The implications of a real power transient spike was not addressed in either of the control method tests, but depending on the EMS designed protective features, the transient could be of concern. Upon completion of the 0.1 s transient, the EMS recovered and almost instantly obtained unity pf.

In addition to the real power spike, reactive power responded to the transient with an initial spike and an overshoot before returning to zero volt-ampere reactive (VAR). This overshoot occurred for both testing parameters listed in Table 2 with a delta of -64.8 VAR's for Test 1 and a delta of -123.09 VAR's for Test 2. Clearly, the RMS control scheme recovered more rapidly and did not overshoot as much as the IRP (αβ) control scheme. With this type of system response for a given transient, pf is reduced due to the additional

VAR’s being inserted by the EMS. It is clear that the EMS reacted to the transient for both real and reactive power.

The unity pf and transient test were designed to evaluate both control schemes for feasibility and implementation. The two unique tests showed minimal differences between either control schemes. Final conclusions and future work are addressed in the next chapter.

V. CONCLUSION AND FUTURE WORK

A. CONCLUSION

The research presented in this thesis focused on a microgrid SIMULINK model that was used to study reactive power control and served as a test platform. The two methods chosen for reactive control in a microgrid were the RMS and the IRP (αβ) theory. The RMS method relied on principles derived from the power triangle, whereas the IRP (αβ) theory is a control method generally applied to three-phase systems. In creating a secondary imaginary orthogonal circuit, this control method can be applied to a single-phase system. Once both methods were designed and implemented in SIMULINK, the model behaved as expected for real power. Both control methods were nearly identical in providing reactive power compensation to create unity pf given a user defined inductive load; however, fewer computations were required for the RMS control method which would save both time and costs in a digital algorithm code structure. Some differences were observed while conducting transient type testing but had negligible impact on overall operational of the EMS. This testing proved useful in determining load tolerances and specification required for various microgrid applications.

B. FUTURE WORK

While conducting research for this endeavor, multiple discussions and ideas were discovered for future work. The importance of this topic continues to grow as advancements are made in power electronics and as the DON explores ways to minimize energy costs.

The models and simulations were analyzed using ideal components. As the models have been verified in this thesis research, analysis can be conducted with parameters that are more representative and time delays to simulate non-ideal conditions. In addition to non-ideal components, exploration into multiple DG sources and analysis in islanding mode is relative and needed for DOD initiatives outlined in [7].

THIS PAGE INTENTIONALLY LEFT BLANK

APPENDIX. MATLAB SCRIPTS

```
% CDR Chris Mendoza, Thesis
% With assistance from:
% NPS Prof. Giovanna Oriti
% NPS Prof. Roberto Cristi
% Dr. Alexander Julian



%Simulation run times*******
tstep = 2e-6;
tstop= .8; %1.5
%**************************

%User inputs for parallel load
%when connected***************
Test_Inductor = .025;
Test_Resistor = 1;
%**************************

% Microgrid parameters*******
Kp_v=.0005; %adjustable gains
Ki_v=.05; %adjustable gains
sw_freq=15000;
vo_ref=120*sqrt(2)*2/pi;
turns= 1; %turns for xformer if desired
Rload=10;
Cap=5e-6;
Lin=1e-3;  %includes the leakage inductance of the 60Hz xfmr, which is
3mH
PWM_mode=0;   %set to one for bipolar PWM or zero for unipolar PWM


% Boost and Buck IC************************
Vbus_ref = 200;
Lboost=150*10^-6;
Lbuck=Lboost;
CapBoost=470*10^-6; % increase *2  when  Rload=26
RloadB= 148/2 ;
slope_compensation = 0;
%Rload= 70 ;    %  to simulate higher power
Vbatt = 72; % V
sw_freqB=15000;
Kp_vB= 6;
Ki_vB=5*2*15;
flpf=7000;
KA=25*4;
gain_dq=-1/2/pi/60;
Kp1=.003;
Ki1=.08;
```

```
%User Inputs*********************************
theta=70*pi/180 %Desired theta
pf=cos(theta)   %PF calc
mag=12          %Magnitude of Sine
z=mag*(cos(theta) + j*sin(theta)) %imped calc
S=(120*sqrt(2))^2/conj(z) %app. power calc
L2=imag(z)/2/pi/60 %calc. L
R2=real(z) %Calc R
%*****************************************


% CDR Chris Mendoza, Thesis
% With assistance from:
% NPS Prof. Giovanna Oriti
% NPS Prof. Roberto Cristi
% Dr. Alexander Julian

%SIMULINK run and plot

clear all;
close all;
mode=0;  % 1 for rms and 0 for AB

%Create file and save for plotting
sim test_10_April_final
PQ_AB = data_PQ;
data_rms_vars_AB=data_rms_vars;
save('PQ.mat','PQ_AB','data_rms_vars_AB');

%Plots of output voltage and current for RMS scheme
figure(1)
subplot(2,1,1), plot(time,vac,'b')
hold on;
subplot(2,1,1), plot(time,iac*10,'r')
hold off;
legend('vac (v)','iac*10 (i)','location','best');
xlabel('time (s)')
ylabel('vac (v) and iac*10 (i)')
%axis([0.7 0.701 14 16])
ylim([-500 500]);
grid
subplot(2,1,2), plot(time,vac,'b')
hold on;
subplot(2,1,2), plot(time,i_ems*10,'r')
hold off;
legend('vac (v)','iems*10 (i)','location','best');
xlabel('time (s)')
ylabel('vac (v) and iems*10 (i)')
%axis([0.7 0.701 0 1.5])
ylim([-500 500]);
grid

% Scenario for IRP scheme
clear all;
```

```
%close all;
mode=1;  % 1 for rms and 0 for AB

%Create file and save for plotting
sim test_10_April_final
PQ_rms = data_PQ;
data_rms_vars_rms=data_rms_vars;


%Plots of output voltage and current for IRP scheme
figure (2)
subplot(2,1,1), plot(time,vac,'b')
hold on;
subplot(2,1,1), plot(time,iac*10,'m')
hold off;
legend('vac (v)','iac*10 (i)','location','best');
xlabel('time (s)')
ylabel('vac (v) and iac*10 (i)')
%axis([0.7 0.701 14 16])
ylim([-500 500]);
grid
subplot(2,1,2), plot(time,vac,'b')
hold on;
subplot(2,1,2), plot(time,i_ems*10,'m')
hold off;
legend('vac (v)','iems*10 (i)','location','best');
xlabel('time (s)')
ylabel('vac (v) and iac*10 (i)')
%axis([0.7 0.701 0 1.5])
ylim([-500 500]);
grid

save('PQrms.mat','PQ_rms','data_rms_vars_rms');
%%
load PQ.mat;
load PQrms.mat;
figure(100)
subplot(2,1,1), plot(time,PQ_AB(:,1),'LineWidth',2);
%xlim([0 1.4]);
hold on;
subplot(2,1,1), plot(time,PQ_rms(:,1),'LineWidth',2);
%xlim([0 1.4]);
hold off;
legend('AB','RMS');
title("P (W)");
xlabel('time (s)');
ylabel('P(W)');
grid;
subplot(2,1,2), plot(time,PQ_AB(:,2),'LineWidth',2);
%xlim([0 1.4]);
hold on;
subplot(2,1,2), plot(time,PQ_rms(:,2),'LineWidth',2);
%xlim([0 1.4]);
hold off
legend('AB','RMS');
```

```
title("Q (VAR)");
xlabel('time (s)')
ylabel('Q(VAR)')
grid;
print(gcf,'-djpeg','-r350','figure1');
figure(101)
subplot(2,1,1), plot(time,PQ_AB(:,2));
hold on;
subplot(2,1,1), plot(time,data_rms_vars_AB);
hold off;
title('Q (VAR)computed two different ways for AB control');
legend('using AB eq.','using RMS eq.');
grid;
subplot(2,1,2), plot(time,PQ_rms(:,2));
hold on;
subplot(2,1,2), plot(time,data_rms_vars_rms);
hold off;
title('Q (VAR) computed two different ways for RMS control');
legend('using AB eq.','using RMS eq.');
grid;
print(gcf,'-djpeg','-r350','figure2');
```

LIST OF REFERENCES

[1] "How the electricity grid works," Union of Concerned Scientists (UCS), 2015, [Online]. Available: http://www.ucsusa.org/clean-energy/how-electricity-grid-works#

[2] National Academy of Sciences, National Academy of Engineering, National Research Council of the National Academies, *America's Energy Future: Technology and Transformation*. Washington, DC, USA: The National Academies Press. [Online]. Available: https://www.nap.edu/read/12091/chapter/1

[3] D. Ton and M. Smith, "The U.S. Department of Energy's microgrid initiative," *The Electricity Journal,* vol. 25, no. 8, pp. 84–94, Oct. 2012. [Online]. Available: https://www.energy.gov/sites/prod/files/2016/06/f32/The%20US%20Department%20of%20Energy%27s%20Microgrid%20Initiative.pdf

[4] G. Oriti, and A. L. Julian, "Reactive power control with an energy management system in single phase AC microgrids," presented at 2015 IEEE Energy Conversion Congress and Exposition (ECCE), Montreal, Canada, Sept. 20–24, 2015. [Online]. Available: https://www.semanticscholar.org/paper/Reactive-power-control-with-an-energy-management-in-Oriti-Julian/29eba26df5684446385b9036fe385b7241b49c44

[5] "Navy bases," United States Navy. Accessed November 1, 2017. [Online]. Available: https://www.navy.com/about/locations/bases.html

[6] "Navy shore energy program," Commander, Navy Installations Command, April 5, 2018. [Online]. Available: https://www.cnic.navy.mil/om/base_support/facility_system_investment/Navy_Shore_Energy_Program.html

[7] "*Shore Energy Management,*" OPNAV Instruction 4100.5E, Office of the Chief of Naval Operations, Washington, DC, USA, 2017.

[8] R. H. Lasseter and P. Paigi, "Microgrid: a conceptual solution," Presented at 2004 IEEE 35th Annual Pwr. Elec. Spec. Conf., Aachen, Germany, Jun. 20–25, 2004. [Online]. Available: http://ieeexplore.ieee.org/document/1354758/

[9] D. V. McGinn, "Microgrids: Macro benefits for our Navy bases," *Navy Live*, May 2, 2016. [Online]. Available: http://navylive.dodlive.mil/2016/05/02/microgrids-macro-benefits-for-our-navy-bases/

[10] J. St. John, "How the military microgrids could save the country," GTM, January 17, 2017. [Online]. Available: https://www.greentechmedia.com/articles/read/amidst-energy-insecurity-a-call-for-military-microgrids#gs.3zX5mbk

[11] A. Burger, "Global microgrid market to grow 21%, exceed $35B by 2020," Microgrid Media, January 6, 2016. [Online]. Available: http://microgridmedia.com/global-microgrid-market-to-grow-21-exceed-35b-by-2020/

[12] F. Valencia, J. Collado, D.Saez, and L.G. Marin, "Robust energy management system for a microgrid based on a fuzzy prediction interval model," in *IEEE Transactions on Smart Grid,* vol. 7, pp. 1483-1494, 2016.

[13] P. Wang, J. Xiao, L. Setyawan, and C.F. Hoong, "Energy management system (EMS) for real-time operation of DC microgrids with multiple slack terminals," in *IEEE Power and Energy Society Innovation Smart Grid Technologies Conference Europe,* Istanbul, Turkey, 2014, pp. 1-6.

[14] R. BiYing, T. XiangQian, S. XiangDong, and Z. Qi, "Research on the control strategy of energy management systems for low capability microgrid," in *IEEE Power Engineering and Automation Conference,* 2011. pp. 441–444.

[15] D. N. Zmood, D.G. Holmes, "Stationary frame current regulation of PWM inverters with zero steady-state error," in *IEEE Transactions on Power Electronics,* vol. 18, pp. 514–822, 2003.

[16] R. Zhang, M. Cardinal, P. Szczesny, and M. Dame, "A grid simulator with control of single-phase power converters in D-Q rotating frame," in *IEEE Power Electronics Specialist Conference,* vol. 3, pp. 1431-1436, 2002.

[17] Y.Y Tzou, R.S. Ou, S.L. Jung, and M.Y. Chang, "High-performance programmable AC power source with low harmonic distortion using DSP-based repetitive control technique," in *IEEE Transaction on Power Electronics,* vol. 12, pp. 715–722, 1997

[18] M.J. Ryan, W.E. Brumsickle, and R.D. Lorenz, "Control topology options for single-phase UPS inverters," in *IEEE Transactions on Industry Applications,* vol. 33, pp. 493-501, 1997.

[19] M.T. Haque and T. Ise, "Implementation of single-phase pq theory," in *IEEE PCC Conference Rec.,* pp. 761–765, 2002.

[20] P.Wang., J. Xiao, L. Setyawan, and C.F. Hoong, "Energy management system (EMS) for real-time operation of DC microgrids with multiple slack terminals," in *IEEE Pow. and Energy Society Innov. Smart Grid Tech. Conf.,* 2014, pp.1-6.

[21] R. BiYing, T. XiangQian, S. XiangDong, and Z. Qi, “Research on the control strategy of energy management system for low capability microgrid,” in *IEEE Pow. Eng. and Auto. Conf.,* 2011, pp. 441-445.

[22] “Power Electronics,” class notes for ECE-4150 Advanced Solid State Power Conversion, Dept. of Electrical and Computer Engineering, Naval Postgraduate School, Monterey, CA, USA, winter 2017.

[23] N. Mohan, T.M. Undeland, and W.P. Robbins, *Power Electronics*. Hoboken, NJ, USA: John Wiley and Sons, 2003.

[24] R. I. Bojoi, L. R. Limongi, D. Roiu and A. Tenconi, "Enhanced power quality control strategy for single-phase inverters in distributed generation systems,” in *IEEE Trans on Pwr Elect Conf.,* 2011, pp. 798-806.

[25] R.I. Bojoi, G. Griva, V. Bostan, M. Guerriero, F. Farnia, and F. Profumo, “Current control strategy for power conditioners using sinusoidal signal integrators in synchronous reference frame,” *IEEE Trans. Pwr Elec.,* 2005, pp. 1402-1412.

[26] P. Rodriguez, R. Teodorescu, I. Candela, A.V. Timbus, M. Lisserre, and F. Blaabjerg, “New positive-sequence voltage detector for grid synchronization of power converters under faulty grid conditions,” in *Proc. IEEE Pwr. Elec. Spcs. Conf.,* 2006, pp. 1-7.

THIS PAGE INTENTIONALLY LEFT BLANK

INITIAL DISTRIBUTION LIST

1. Defense Technical Information Center
   Ft. Belvoir, Virginia

2. Dudley Knox Library
   Naval Postgraduate School
   Monterey, California